


ARTICLE

CEP55 promotes cilia disassembly through stabilizing Aurora A kinase

Yu-Cheng Zhang^{1*}, Yun-Feng Bai^{1*}, Jin-Feng Yuan¹, Xiao-Lin Shen¹, Yu-Ling Xu¹, Xiao-Xiao Jian¹, Sen Li¹, Zeng-Qing Song¹, Huai-Bin Hu¹, Pei-Yao Li^{1,3}, Hai-Qing Tu¹, Qiu-Ying Han¹, Na Wang¹, Ai-Ling Li¹, Xue-Min Zhang¹, Min Wu¹, Tao Zhou¹, and Hui-Yan Li^{1,2} 

Primary cilia protrude from the cell surface and have diverse roles during development and disease, which depends on the precise timing and control of cilia assembly and disassembly. Inactivation of assembly often causes cilia defects and underlies ciliopathy, while diseases caused by dysfunction in disassembly remain largely unknown. Here, we demonstrate that CEP55 functions as a cilia disassembly regulator to participate in ciliopathy. *Cep55*^{−/−} mice display clinical manifestations of Meckel–Gruber syndrome, including perinatal death, polycystic kidneys, and abnormalities in the CNS. Interestingly, *Cep55*^{−/−} mice exhibit an abnormal elongation of cilia on these tissues. Mechanistically, CEP55 promotes cilia disassembly by interacting with and stabilizing Aurora A kinase, which is achieved through facilitating the chaperonin CCT complex to Aurora A. In addition, CEP55 mutation in Meckel–Gruber syndrome causes the failure of cilia disassembly. Thus, our study establishes a cilia disassembly role for CEP55 in vivo, coupling defects in cilia disassembly to ciliopathy and further suggesting that proper cilia dynamics are critical for mammalian development.

Introduction

Primary cilia, emanating from the mother centriole, play a key role in vertebrate development by receiving and integrating extracellular signals, such as Hedgehog (Hh) and Wnt signals (Gerdes and Katsanis, 2008; Kim and Dynlacht, 2013). Primary cilia are assembled in quiescent cells and must be disassembled before entry into mitosis in order to release centrosomes to participate in establishing spindle poles, thus ensuring correct segregation of chromosomes (Liang et al., 2016; Sánchez and Dynlacht, 2016). Thus, timely and accurate cilia disassembly is essential for cell proliferation and differentiation.

Ciliopathy is a class of human diseases that share the etiological factor of defective cilia structure and function (Badano et al., 2006), including Meckel–Gruber syndrome (MKS; Valente et al., 2010; Williams et al., 2011), Bardet–Biedl syndrome (Blacque et al., 2004; Blacque and Leroux, 2006), nephronophthisis (Fliegauf et al., 2006; Won et al., 2011), and polycystic kidney disease (Gogusev et al., 2003; Burtley et al., 2008). MKS, as a perinatally lethal disease, represents a severe form of ciliopathy and is characterized by the presence of malformation of the central nervous system (CNS; Hartill et al., 2017), renal cystic dysplasia, and occipital encephalocele. Many MKS genes are involved in cilia assembly, such as MKS1 (Kyttälä et al., 2006),

TMEM107 (Lambacher et al., 2016), NPHP4 (Won et al., 2011), and CEP290 (Frank et al., 2008). In most cases characterized so far, patients or animal models with ciliopathy display defects in ciliary assembly or functions. Conversely, causative mutations in cilia disassembly have not been widely linked to ciliopathy.

Ciliation can be recapitulated in cell culture through serum starvation, while culture in serum-containing medium induces cilia disassembly. Previous studies have reported that several key signaling pathways can induce cilia disassembly (Liang et al., 2016), such as the Aurora A–HDAC6 (Pugacheva et al., 2007) and Nek2–Kif24 pathways (Kim et al., 2015) and actin polymerization (Ran et al., 2015). Now, it is generally accepted that Aurora A is the major pathway that directly induces deacetylation of ciliary axonemal microtubule by activating HDAC6 (Liang et al., 2016). Intriguingly, in addition to being activated upon phosphorylation, Aurora A is dynamic at protein level during the ciliary cycle. Thus far, intense investigation has focused on Aurora A kinase activation or the transcriptional regulation (Plotnikova et al., 2015), while the mechanisms governing the dynamic regulation of Aurora A protein stability remain unclear.

¹State Key Laboratory of Proteomics, National Center of Biomedical Analysis, Beijing, China; ²School of Basic Medical Sciences, Fudan University, Shanghai, China; ³School of Medicine, Tsinghua University, Beijing, China.

*Y.-C. Zhang and Y.-F. Bai contributed equally to this paper; Correspondence to Hui-Yan Li: hyli@ncba.ac.cn; Tao Zhou: tzhou@ncba.ac.cn; Min Wu: mwu@xmail.ncba.ac.cn.

© 2021 Zhang et al. This article is distributed under the terms of an Attribution–Noncommercial–Share Alike–No Mirror Sites license for the first six months after the publication date (see <http://www.rupress.org/terms/>). After six months it is available under a Creative Commons License (Attribution–Noncommercial–Share Alike 4.0 International license, as described at <https://creativecommons.org/licenses/by-nc-sa/4.0/>).

CEP55 (centrosomal protein of 55 kD) localizes to the centrosome in interphase and to the midbody in cytokinesis (Fabbro et al., 2005; Martinez-Garay et al., 2006). The well-established function of CEP55 at the midbody is to orchestrate cell membrane abscission (the final step of cytokinesis) by regulating the endosomal sorting complex required for transport (ESCRT) complex (Carlton and Martin-Serrano, 2007; Carlton et al., 2008; Lee et al., 2008; Morita et al., 2010; Green et al., 2012). In contrast, the function of CEP55 as a centrosome protein in interphase remains to be addressed. Recently, a homozygous nonsense mutation (c.256C>T) in the CEP55 gene has been linked to human MKS (Bondeson et al., 2017), but whether and how this CEP55 mutation causes MKS is unclear.

In this study, we show that *Cep55*^{-/-} mice display clinical symptoms of MKS, including postnatal lethality, hydrocephalus, ventriculomegaly, and polycystic kidneys. These *Cep55*^{-/-} mice display long cilia in the brains, neural tubes, and kidneys. Next, we demonstrated that CEP55 negatively regulates cilia formation through promoting cilia disassembly. Our study indicates that mutation of CEP55 and abnormal cilia disassembly can cause MKS and suggests that dynamic regulation of cilia formation is crucial to vertebrate development.

Results

Cep55^{-/-} mice exhibit Meckel–Gruber syndrome phenotypes and elongated primary cilia

To explore the physiological functions of Cep55 in vivo, we generated homozygous *Cep55*^{-/-} mice (Fig. S1, A and B). Immunoblot analysis of primary mouse embryonic fibroblasts (MEFs) confirmed the absence of Cep55 protein (Fig. S1, C and D). These *Cep55*^{-/-} mice were born at the normal Mendelian ratio but suffered 100% (21/21) mortality before postnatal day 2 (P2; Table S1). Thus, complete inactivation of Cep55 led to postnatal death in mice. As perinatal death is a characteristic of MKS (Hartill et al., 2017), we next tested the other clinical features of *Cep55*^{-/-} mice before their lethality.

The biggest characteristic of human MKS is the malformation of the CNS (Hartill et al., 2017). Magnetic resonance imaging (MRI) analysis revealed obvious hydrocephalus and ventriculomegaly in *Cep55*^{-/-} embryos at embryonic day 18.5 (E18.5; Fig. 1A). Histological analysis of E18.5 and E14.5 *Cep55*^{-/-} embryos revealed obvious dilations of the lateral ventricles, the third ventricle, and the dorsal third ventricle (Fig. 1, B and C). In addition to ventricle enlargement, the third ventricle and dorsal third ventricle were merged into one large ventricle in *Cep55*^{-/-} embryos (Fig. 1B, right). During the perinatal period, the brain choroid plexus epithelial cells (CPECs) form one or two dozen nonmotile 9+0 primary cilia (Narita and Takeda, 2015). The impaired cilia function of CPECs has been reported to lead to neonatal hydrocephalus with dilation of the brain ventricles in mice (Banizs et al., 2005; Spassky et al., 2005; Tissir et al., 2010; Vogel et al., 2012). Thus, we next examined cilia formation in wild-type and *Cep55*^{-/-} CPECs (pups at P0.5) by staining with the ciliary marker polyglutamylated tubulin (GT335). The results showed that most wild-type CPECs have normal cilia clusters on the apical surface, while *Cep55*^{-/-} CPECs exhibited abnormally

elongated cilia (Fig. 1D). Compared with 1.13 μm in wild-type CPECs, the mean cilium length increased to 2.20 μm in *Cep55*^{-/-} CPECs (Fig. 1E).

The above histological data also showed that *Cep55*^{-/-} brains at E18.5 display CNS malformation, including thinner cortex, constricted hippocampus, and severe deformations in caudate putamen (striatum) and thalamus (Fig. 1B). Since cerebellar hypoplasia is another hallmark of MKS (Ahdab-Barmada and Claassen, 1990; Aguilar et al., 2012; Hong and Hamilton, 2016), we also quantified the size of cerebellum and found that *Cep55*^{-/-} mice displayed an extremely smaller cerebellum than wild type (Fig. 1, F and G). Given that primary cilium in the neural tube at early embryo development is essential for the ultimate formation of CNS (Paridaen et al., 2013), we next examined cilia morphology in the neural tube at E9.5. Compared with wild-type mice, we observed enlarged cilia with obvious bulges at their bases and shafts by scanning electron microscopy in *Cep55*^{-/-} neural tubes (Fig. 1H). These data suggested that the abnormal cilia in neural tubes might be the cause of CNS malformation in *Cep55*^{-/-} mice.

Since cystic dysplasia of the kidneys is also frequently observed in MKS patients (Hartill et al., 2017), we further performed the renal histological examination. We observed multiple microscopic cysts at the glomeruli and renal tubules of *Cep55*^{-/-} kidneys (Fig. 1I). Meanwhile, primary cilia of renal tubular epithelial cells in *Cep55*^{-/-} embryos were much longer as compared with those in wild-type embryos (Fig. 1, J and K). Taken together, *Cep55*^{-/-} mice exhibited highly canonical phenotypes of the cerebral and renal malformation (Fig. 1L), which were also observed in human MKS fetuses with CEP55 mutation (Bondeson et al., 2017; Rawlins et al., 2019). Thus, these results indicated that Cep55 deletion causes elongated primary cilia and contributes to Meckel–Gruber syndrome phenotypes.

Furthermore, we performed histological analysis of some other tissues, such as faces and limbs (which are also recognized as affected tissues in MKS) and did not find remarkable abnormalities in these tissues from *Cep55*^{-/-} mice (Fig. S1, E and F). We subsequently analyzed the cilia formation in above tissues by staining ARL13B as a ciliary marker. Interestingly, *Cep55*^{-/-} mice do not display obvious increase in cilia number or length in facial mesenchyme and limbs (Fig. S1, G and H), which is consistent with the phenotypes in CEP55-mutated human fetuses, none of whom displayed polydactyly or facial malformation as previously reported (Bondeson et al., 2017). Thus, Cep55 is required for normal cilia formation in many, but not all, tissues.

Cep55 deficiency induces cell cycle arrest and decreased Smoothened (Smo) enrichment by abnormal cilia

Next, we test the cilia formation in primary MEFs. Our data showed that less than 15% of wild-type MEFs formed cilia in the presence of serum, whereas ~50% of *Cep55*^{-/-} MEFs exhibited cilia formation (Fig. 2, A and B). This result suggests that Cep55 deficiency increased the percentage of cilia in MEFs. Meanwhile, primary cilia in *Cep55*^{-/-} MEFs were much longer than those in wild-type MEFs after serum starvation (Fig. 2, C and D). Therefore, these findings indicated that Cep55 regulates proper ciliogenesis in vivo.

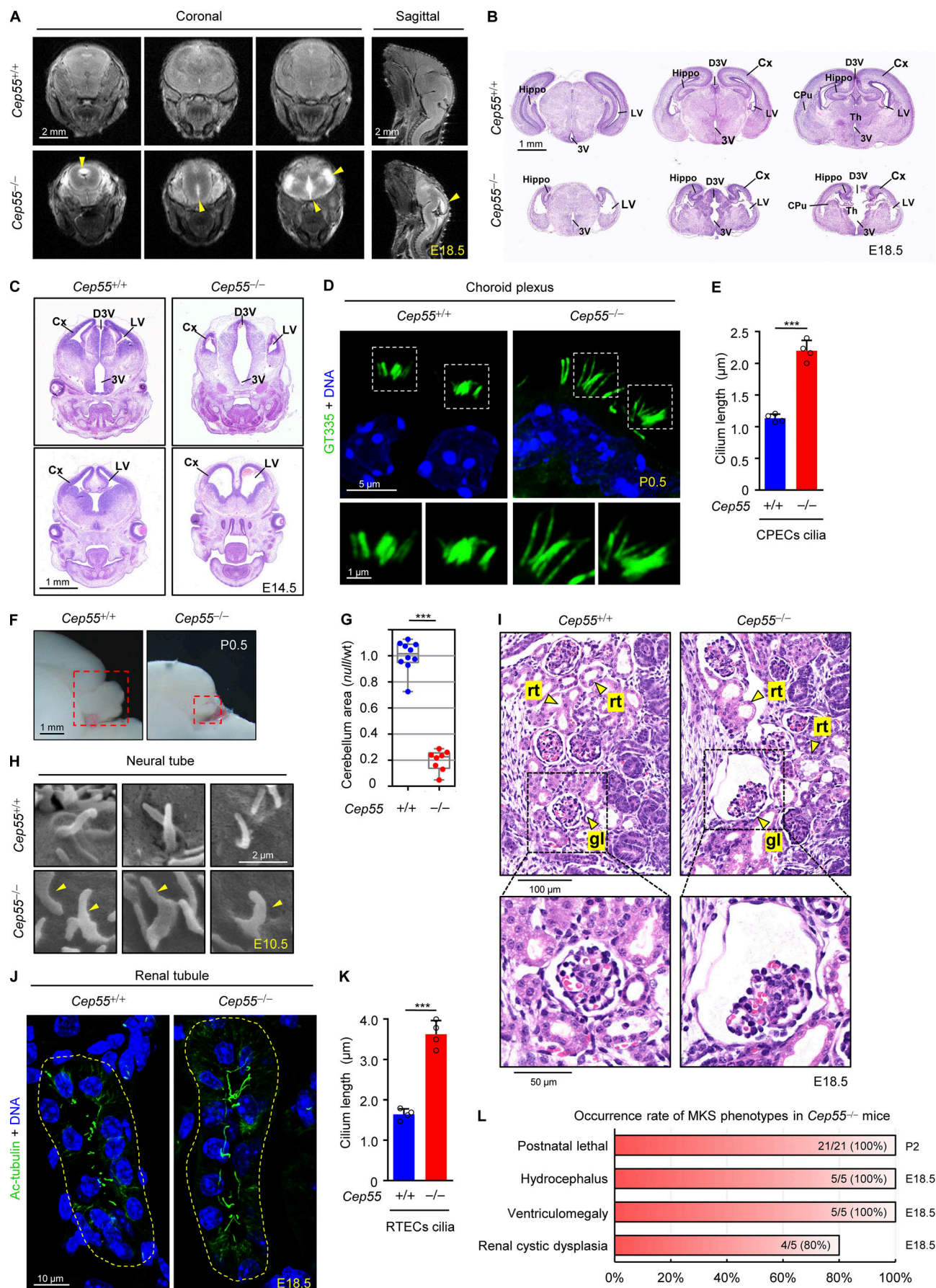


Figure 1. *Cep55*^{-/-} mice exhibit Meckel–Gruber syndrome phenotypes and elongated primary cilia. (A) Coronal and sagittal MRI of *Cep55*^{+/+} and *Cep55*^{-/-} heads at E18.5. Arrowheads indicate hydrocephalus and ventricle dilatations in *Cep55*^{-/-} embryos compared with the morphology in wild-type embryos. Scale bars, 2 mm. **(B and C)** E14.5 and E18.5 coronal sections from anterior to posterior through heads and brains, respectively. 3V, third ventricle; CPU, caudate putamen; Cx, cortex; D3V, dorsal third ventricle; Hippo, hippocampus; LV, lateral ventricle; Th, thalamus. Scale bars, 1 mm. **(D)** P0.5 *Cep55*^{+/+} and *Cep55*^{-/-} CPECs were stained with the ciliary marker (GT335, green) and DNA (blue). Insets show zoomed-in views of the boxed regions. Scale bars, 5 μ m (main image) and 1 μ m (magnified region). **(E)** Quantitative analysis of the cilium length in D (four mice per group). **(F)** Representative images of mid-sagittal view of the brain from *Cep55*^{+/+} and *Cep55*^{-/-} littermates at P0.5. The dashed boxes indicate cerebellum. Scale bar, 1 mm. **(G)** The ratio of midline cerebellum area (*null*/wild type [*wt*]) quantified in ImageJ software from *Cep55*^{+/+} and *Cep55*^{-/-} littermates (four mice per group). **(H)** Scanning electron micrographs show that primary cilia in E10.5 *Cep55*^{-/-} neural tube are bulged at the bases and shafts of cilia (arrowheads). Scale bar, 2 μ m. **(I)** E18.5 transverse sections of the kidneys from *Cep55*^{+/+} and *Cep55*^{-/-} littermates were stained with hematoxylin and eosin. gl, glomerulus; rt, renal tubule. Insets show zoomed-in views of the boxed regions. Scale bars, 100 μ m (main image) and 50 μ m (magnified region). **(J)** E18.5 *Cep55*^{+/+} and *Cep55*^{-/-} kidney sections were stained with the ciliary marker (Ac-tubulin, green) and DNA (blue). The dashed circles indicate renal tubules. Scale bar, 10 μ m. **(K)** Quantitative analysis of the cilium length in H (four mice per group). **(L)** Summarized and quantified results of four main MKS phenotypes in *Cep55*^{-/-} mice at P2 or E18.5. Data are means \pm SD of three independent experiments in E, G, and K. An unpaired two-tailed *t* test was performed. ***, *P* < 0.001.

In quiescent cells, the mother centriole can convert to basal body that allows ciliary axoneme formation. Before cell cycle reenters, primary cilium must be disassembled in order to release centrosomes to form spindle poles during mitosis (Liang et al., 2016; Sánchez and Dynlacht, 2016). We thus tested whether abnormal cilia induced by *Cep55* deficiency is associated with cell cycle arrest. Consistent with above data, *Cep55*^{-/-} MEFs exhibited a significant increase in ciliation and a decrease in the percentage of EdU-incorporated cells, indicating that *Cep55* deficiency induced G1 phase arrest (Fig. 2, E and F). Since Ift20 is a key intraflagellar transport (Ift) protein required for cilia maintenance and formation (Follit et al., 2006), we knocked down of *Ift20* to abolish the cilia formation in *Cep55*^{-/-} MEFs. Importantly, codepletion of *Ift20* also released G1 phase arrest caused by *Cep55* deletion and allowed EdU incorporation (Fig. 2, E and F). The efficiency in *Cep55* and *Ift20* depletion was determined by immunoblotting (Fig. 2 G). Collectively, these data suggest that abnormal ciliation caused by *Cep55* deficiency contributes to cell cycle arrest. Further FACS analysis showed that *Cep55* deficiency mainly arrested cell at the G0/G1 phase and did not increase the percentage of multinucleated cells (Fig. 2, H and I). Taken together, these results suggested that cell cycle arrest in *Cep55*^{-/-} MEFs is most likely caused by abnormal cilia formation instead of deficient cytokinesis in cancer cells (Fabbro et al., 2005; Martinez-Garay et al., 2006).

To better understand the function of *Cep55* in cell cycle in vivo, we examined cell proliferation in the brains by assessing Ki67 expression, which marks cells in all phases of the cell cycle except G0 phase. Quantification of Ki67 expression revealed that *Cep55*^{-/-} mice had a 55% reduction in cell proliferation in P0.5 cerebral cortex compared with wild-type mice (Fig. 2, J and K), which was in accordance with the thinner cortex shown before (Fig. 1 B). To figure out whether decreased proliferation is due to aberrant mitosis in *Cep55*^{-/-} cortex, we detected mitotic marker phospho-histone H3 (p-H3) in the cortical sections. Immunostaining revealed that there was little decline in the number of p-H3-positive cells per unit ventricular length in *Cep55*^{-/-} cortices (Fig. S2, A and B). We note that these data probably supported that *Cep55* deficiency mainly arrested cell at the G0/G1 phase, but not mitosis, consistent with the data in *Cep55*^{-/-} MEFs.

Furthermore, primary cilia are critical for transduction of several extracellular signals, most notably Hh signals during

embryonic neurogenesis (Goetz and Anderson, 2010). Binding of Hh ligand to its receptor *Ptch1* allows Smo protein accumulation at the cilia to activate the downstream pathway, which is responsible for both cell fate and growth in the developing CNS (Rowitch et al., 1999; Youn and Han, 2018). To investigate whether Hh signaling is affected in *Cep55*^{-/-} mice, we analyzed the localization of Smo protein to cilia in SAG (Smo agonist)-treated cells. In response to SAG treatment, Smo localized to cilia in wild-type MEFs, but not to cilia in *Cep55*^{-/-} MEFs (Fig. 2, L and M). Together, these results indicate that *Cep55* deficiency resulted in decreased Smo enrichment, which possibly led to defect in Hh signal transduction. Our mice model provides more evidence for a fundamental role of CEP55 during embryogenesis and development of disease.

Depletion of CEP55 increased the percentage and length of primary cilia in cultured cells

To further confirm the role of CEP55 in cilia formation, we knocked down CEP55 in RPE-1 cells using three individual siRNA against CEP55. The percentage of ciliated cells was highly increased in CEP55-depleted cells compared with control cells in the presence of serum (Fig. 3, A–C). Consistent with the data in vivo, CEP55 depletion also greatly increased the length of cilia in the absence of serum in RPE-1 cells (Fig. 3, D and E). Furthermore, our data showed that depletion of CEP55 does not destroy the integrity of the centrosome (Fig. S3, A–E).

CEP55 was originally identified as a regulator of cytokinesis. Its function in cytokinesis depends on phosphorylation of multiple residues (S425, S428, and S436), which promote its relocation from the centrosome to the midbody (Fabbro et al., 2005). We verified the endogenous localization of CEP55. Microscopy analysis revealed that CEP55 colocalized with the centrosomal marker γ -tubulin in interphase and went to midbody during cytokinesis (Fig. S3, F–H). We next investigated whether the function of CEP55 in suppressing cilia formation depends on its cytokinesis function. Consistent with endogenous CEP55 localization in interphase, mCherry-CEP55-WT localized to the centrosome and obviously inhibited ciliation in serum-starved RPE-1 cells (Fig. 3, F–H). Similar to CEP55-WT, CEP55 phosphorylation-deficient mutant 3SA (S425A/S428A/S436A) also inhibited cilia formation (Fig. 3, F–H), indicating that the inhibitory effect of CEP55 on cilia formation is independent of its cytokinesis function.

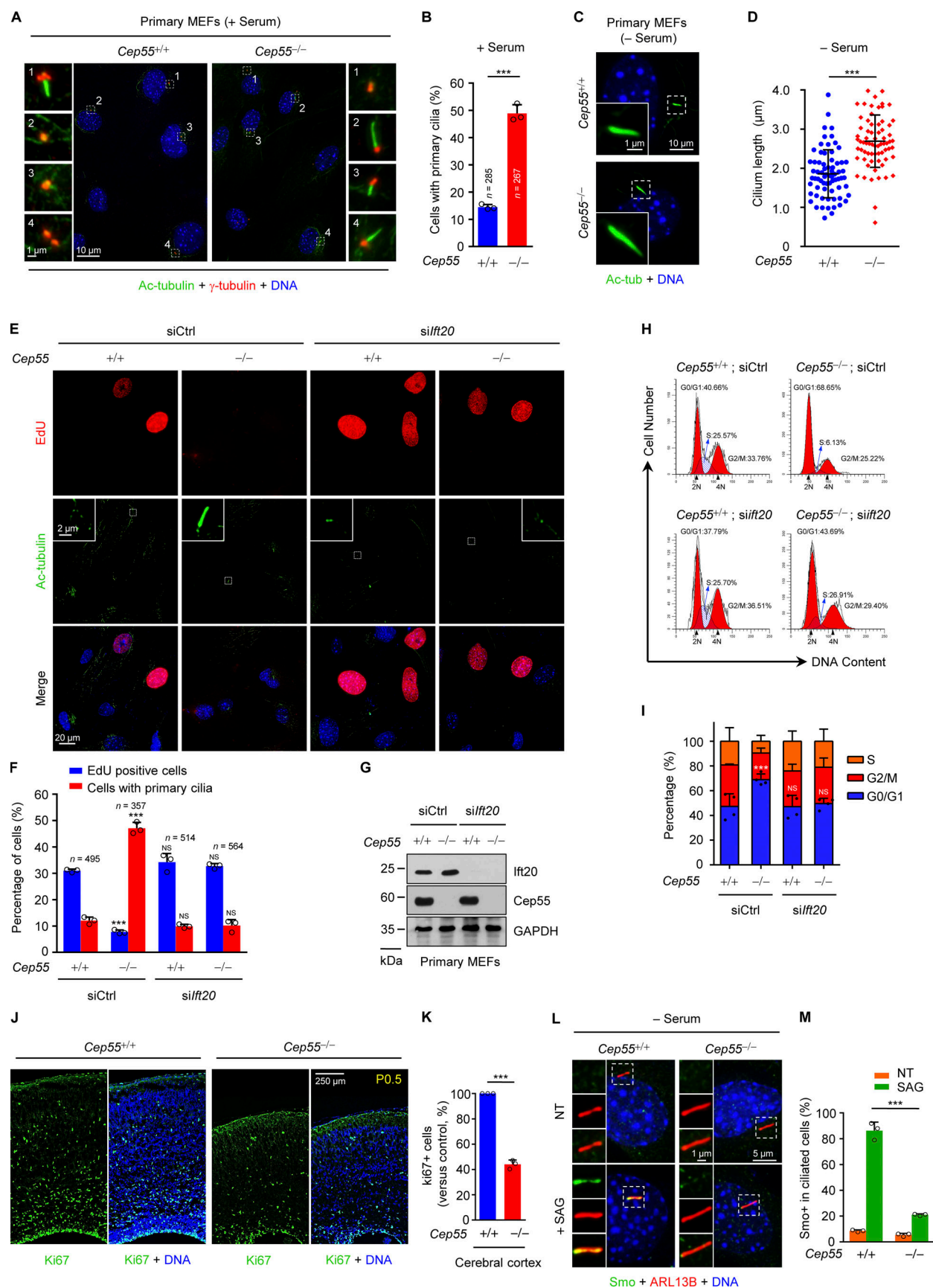


Figure 2. **Cep55** deficiency induces cell cycle arrest and decreased Smo enrichment by abnormal cilia. (A) *Cep55*^{+/+} and *Cep55*^{-/-} primary MEFs were stained with Ac-tubulin (green), a centrosome marker (γ -tubulin, red), and DNA (blue) in the presence of serum (+ Serum). Insets show zoomed-in views of the

boxed regions. Scale bars, 10 μ m (main image) and 1 μ m (magnified region). **(B)** Quantification of the ciliated cells in A (three mice per group). Data are means \pm SD. Unpaired two-tailed *t* test was performed. ***, *P* < 0.001. *n*, number of cells. **(C)** *Cep55*^{+/+} and *Cep55*^{-/-} primary MEFs were stained with Ac-tubulin (green) and DNA (blue) under serum starvation (- Serum). Insets show zoomed-in views of the boxed regions. Scale bars, 10 μ m (main image) and 1 μ m (magnified region). **(D)** Graph showing quantitative analysis of the cilium length in C. Each dot represents one cell. Data are means \pm SD. Unpaired two-tailed *t* test was performed. ***, *P* < 0.001. **(E)** *Cep55*^{+/+} and *Cep55*^{-/-} primary MEFs were transfected with control and *lft20* siRNA and then stained with EdU (red), Ac-tubulin (green), and DNA (blue). Insets show zoomed-in views of the boxed regions. Scale bars, 20 μ m (main image) and 2 μ m (magnified region). **(F)** The percentages of EdU-positive cells and ciliated cells in E were quantified. Data are means \pm SD of three independent experiments. A two-way ANOVA test was performed in each group, followed by Dunnett's multiple comparisons. ***, *P* < 0.001. *n*, number of cells. **(G)** Immunoblot of primary MEFs lysates in (E and F) with the indicated antibodies. **(H)** *Cep55*^{+/+} and *Cep55*^{-/-} primary MEFs were transfected with control and *lft20* siRNA and then stained with propidium iodide for DNA content analysis by FACS. DNA content is represented on the x axis, and the number of cells counted is represented on the y axis. Cell populations in G0/G1, S, and G2/M phases are given as percentage of total cells. **(I)** Graphical representations of the cell cycle distribution of the samples in H. Data are presented as means \pm SD of three independent experiments. One-way ANOVA test was performed to analyze the difference of the percentage of cells in G1 phase in each group followed by Dunnett's multiple comparisons. ***, *P* < 0.001. **(J)** P0.5 *Cep55*^{+/+} and *Cep55*^{-/-} cerebral cortex coronal sections were stained with proliferation marker (Ki67, green) and DNA (blue). Scale bar, 250 μ m. **(K)** Quantification of Ki67-positive (Ki67⁺) cells in the cerebral cortex in J (three mice per group). Data are means \pm SD. An unpaired two-tailed *t* test was performed. ***, *P* < 0.001. **(L)** *Cep55*^{+/+} and *Cep55*^{-/-} primary MEFs treated with SAG in the absence of serum (- Serum) were stained with Smo (green), ARL13B (red), and DNA (blue). Insets show zoomed-in views of the boxed regions. Scale bar, 5 μ m (main image) and 1 μ m (magnified region). **(M)** Quantification of the Smo-positive (Smo⁺) ciliated cell in L. Data are presented as means \pm SD of three independent experiments. A two-way ANOVA test was performed followed by Bonferroni's multiple comparisons. ***, *P* < 0.001. NT, non-treatment.

CEP55 inhibits cilia formation through interacting with Aurora A kinase

We next sought to further explore the mechanism by which CEP55 inhibits cilia formation. We first identified possible CEP55-binding proteins by mass spectrometry (Fig. S4 A) and focused on the protein with centrosomal localization. Interestingly, Aurora A, a major regulator of cilia disassembly, was among these candidates. We confirmed the interaction between Aurora A and CEP55 in HEK293T cells by ectopically expressing Flag-CEP55 (Fig. 4 A). We next tested whether CEP55 was present in the same complex with Aurora A endogenously. We found that only Aurora A efficiently bound CEP55 in HEK293T cells, whereas HDAC6, the substrate of Aurora A, did not interact with CEP55 directly (Fig. 4 B). The endogenous interaction between CEP55 and Aurora A was further confirmed by immunoprecipitation in primary MEFs (Fig. 4 C). Immunofluorescence data showed that CEP55 colocalized with Aurora A, both located at the centrosome (Fig. S4 B). Moreover, after serum stimulation, the colocalization between phospho-Aurora A (T288) and CEP55 at the centrosome can be also detected (Fig. S4 C). Next, we mapped the essential domain of CEP55 required for interaction with Aurora A. Our data showed that the C-terminal region (residues 217–464 and 355–464) of CEP55 could bind to Aurora A, similar to the full length of CEP55 (Fig. 4, D and E). However, the N-terminal region (residues 1–217), residues 217–355, and 1–355 truncation of CEP55 could no longer bind to Aurora A (Fig. 4, D and E). This result suggested that residues 355–464 of CEP55 are critical for binding to Aurora A. Importantly, this C-terminal region (residues 217–464 and 355–464) of CEP55, not its N-terminal region (residues 1–355), efficiently inhibits ciliation induced by serum starvation (Fig. 4 F). Taken together, our results indicate that CEP55 negatively regulates cilia formation, possibly by interacting with Aurora A.

Recently, a nonsense mutation c.256C>T (p.Arg86*) in the CEP55 gene defined a new locus for human MKS (Bondeson et al., 2017). To verify whether this mutation affects the function of CEP55 on cilia formation, we constructed the mCherry-CEP55 C256T mutant (1–85 aa; Fig. 4 G) and examined its effect on cilia formation. Our data showed that CEP55 C256T mutant

could not localize to the centrosome (Fig. 4 H). Consistently, this C256T mutant failed to bind to Aurora A (Fig. 4 I) and cannot rescue increased ciliation induced by CEP55 depletion (Fig. 4, J and K), suggesting that the C256T mutant loses the inhibitory activity on cilia formation. Thus, we speculate that this CEP55 mutation leads to MKS, potentially through deregulating cilia formation.

CEP55 promotes cilia disassembly by regulating Aurora A stability

As Aurora A plays a key role in cilia disassembly, we hypothesized that CEP55 might affect cilia disassembly. To verify this, we induced cilia assembly in RPE-1 cells with serum starvation for 48 h and then stimulated the ciliated cells with serum for 24 h to trigger cilia disassembly (Fig. 5 A). After serum restimulation for 24 h, a dramatic decrease in cilia formation was observed in control RPE-1 cells, whereas CEP55-depleted cells were strongly resistant to serum-induced cilia disassembly (Fig. 5, B and C). Thus, these results suggest that, similar to Aurora A, CEP55 is required for cilia disassembly. We thus tested whether CEP55 promoted cilia disassembly in vivo. Consistent with the effects on RPE-1 cells, after serum restimulation for 24 h, cilia disassembly occurred in the majority of ciliated wild-type primary MEFs, whereas *Cep55*^{-/-} MEFs were resistant to serum-induced cilia disassembly (Fig. 5 D and Fig. S5 A).

Although Aurora A activity is dynamically regulated during the ciliary cycle, protein levels of Aurora A are highly dynamic. To further investigate the mechanism of CEP55 in cilia disassembly, we observed the protein profile of CEP55 and Aurora A during the ciliary cycle. Consistent with a previous report (Pugacheva et al., 2007), total Aurora A levels increased slightly at 2 h and peaked 18–24 h after serum stimulation (Fig. 5 E). Interestingly, we observed the similar protein profile of CEP55 as Aurora A during the ciliary cycle (Fig. 5 E). Importantly, Aurora A protein levels in CEP55-depleted RPE-1 cells were dramatically reduced at 0 and 2 h with serum stimulation and only have a slight increase even after serum stimulation for 18 or 24 h (Fig. 5 F). A similar reduction of Aurora A protein levels was also observed in *Cep55*^{-/-} MEFs during cilia disassembly (Fig. S5 B).

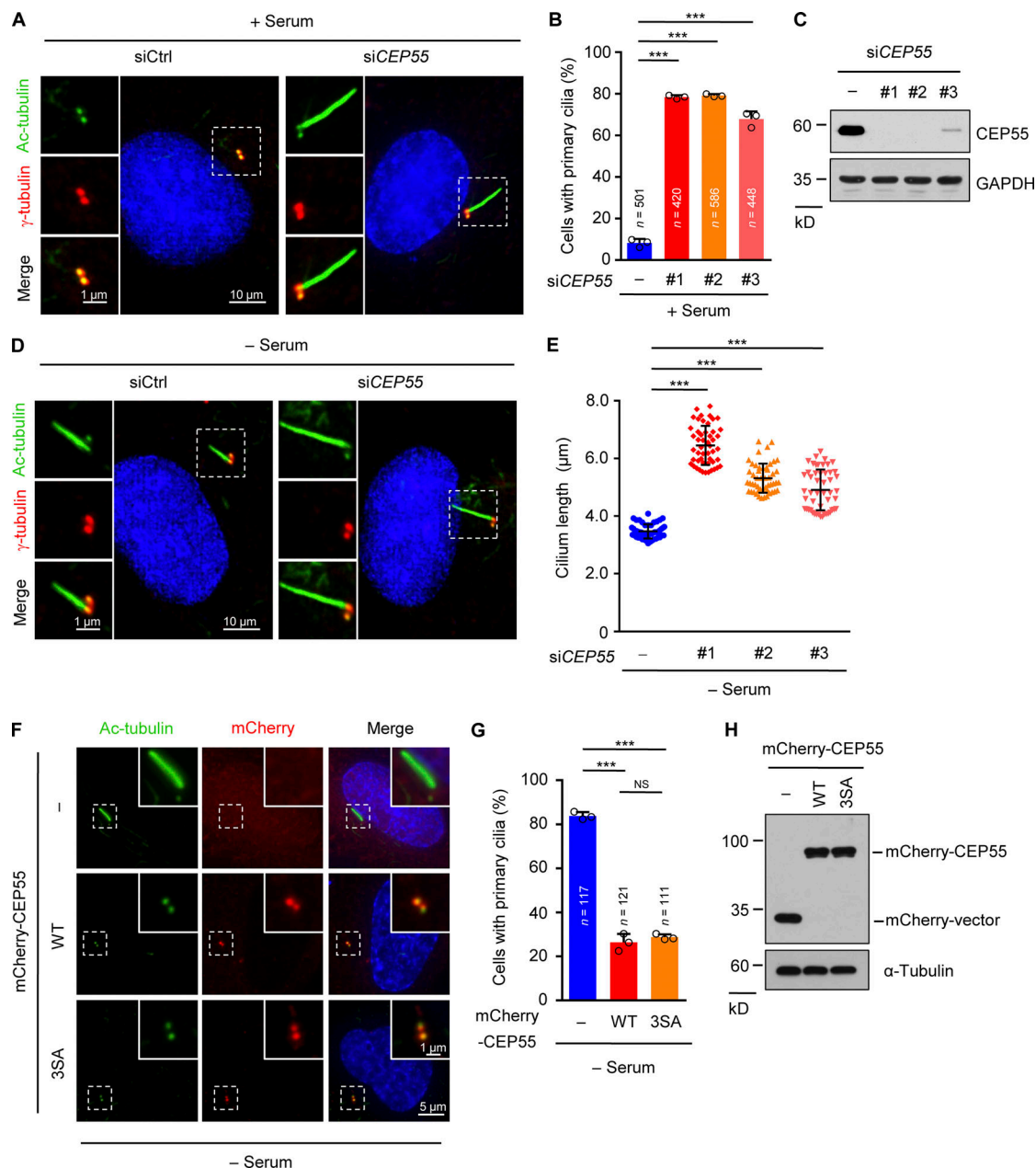
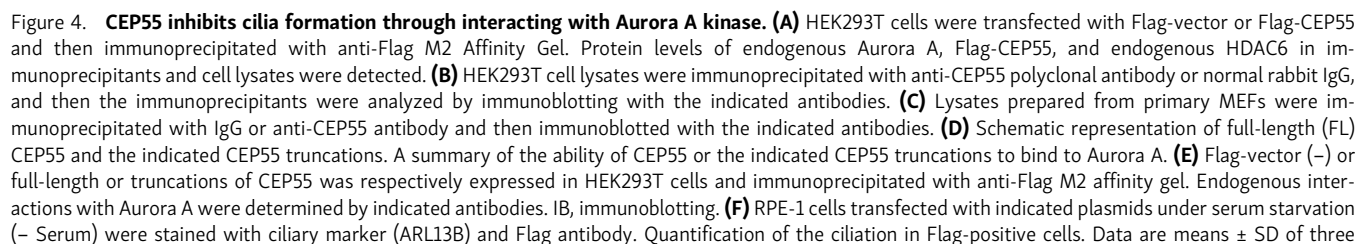


Figure 3. Depletion of CEP55 increases the percentage and length of primary cilia in cultured cells. (A) RPE-1 cells transfected with control or CEP55 siRNA in the presence of serum (+ Serum) were stained with Ac-tubulin (green), γ-tubulin (red), and DNA (blue). Insets show zoomed-in views of the boxed regions. Scale bars, 10 μm (main image) and 1 μm (magnified region). (B) Effects of CEP55 depletion on cilia formation in the presence of serum (+ Serum) in RPE-1 cells. Quantification of the ciliated cells in A with three individual siRNAs against CEP55. Data are means ± SD of three independent experiments. One-way ANOVA test was performed followed by Dunnett's multiple comparisons. ***, $P < 0.001$. n , number of cells. (C) Immunoblot of RPE-1 cells lysates in A and B with the indicated antibodies. (D) RPE-1 cells transfected with control or CEP55 siRNA were stained with Ac-tubulin (green), γ-tubulin (red), and DNA (blue) under serum starvation (- Serum). Insets show zoomed-in views of the boxed regions. Scale bars, 10 μm (main image) and 1 μm (magnified region). (E) Quantitative analysis of the cilium length in D with three individual siRNAs against CEP55. Each dot represents one cell. Data are means ± SD. A one-way ANOVA test was performed followed by Dunnett's multiple comparisons. ***, $P < 0.001$. (F) RPE-1 cells were transfected with mCherry-vector (-), mCherry-CEP55-WT, or mCherry-CEP55 3SA and then starved for 48 h. Cells were stained with Ac-tubulin (green) and DNA (blue). Insets show zoomed-in views of the boxed regions. Scale bars, 5 μm (main image) and 1 μm (magnified region). (G) Quantification of the ciliation in mCherry-positive cells in F. Data are means ± SD of three independent experiments. A one-way ANOVA test was performed. ***, $P < 0.001$. n , number of cells. (H) Immunoblot of RPE-1 cells lysates in F and G with the indicated antibodies.

Furthermore, our data showed that total Aurora A levels decreased in E9.5 neural tubes from *Cep55*^{-/-} mice compared with wild-type mice (Fig. S5 C). Thus, we speculate that *Cep55*-deficient mice induced abnormal cilia formation, likely through

destabilizing Aurora A protein. Meanwhile, expression of Aurora A mRNA was hardly decreased in CEP55-depleted RPE-1 cells (Fig. 5 G), suggesting that CEP55 stabilizes Aurora A at the protein level during the ciliary cycle. These data showed that the



independent experiments. A one-way ANOVA test was performed, with each mean compared with the Flag-CEP55 group, followed by Dunnett's multiple comparisons. ***, $P < 0.001$. *n*, number of cells. **(G)** Schematic diagram of CEP55 C256T mutant in human MKS (c.256C>T, p.Arg86*). **(H)** The nonsense mutation C256T in CEP55 abolished its centrosome localization. RPE-1 cells transfected with mCherry-CEP55-WT or C256T mutant were stained with γ -tubulin (green) and DNA (blue). Insets show zoomed-in views of the boxed regions. Scale bars, 5 μ m (main image) and 0.5 μ m (magnified region). **(I)** HEK293T cells were cotransfected with HA-Aurora A together with mCherry-vector (–), mCherry-CEP55-WT, or C256T mutant. Lysates were immunoprecipitated with anti-HA Agarose antibody, and then immunoprecipitants and whole-cell lysates were analyzed by immunoblotting with indicated antibodies. **(J)** Increased ciliation caused by CEP55 depletion can be rescued by the expression of an RNAi-resistant mCherry-CEP55 WT, but not by C256T mutant. RPE-1 cells were transfected with the indicated siRNA and plasmids (– indicates mCherry-vector) and then stained with Ac-tubulin (green) and DNA (blue). Insets show zoomed-in views of the boxed regions. Scale bars, 5 μ m (main image) and 1 μ m (magnified region). **(K)** Quantification of the ciliation in mCherry-positive cells in G. Data are presented as means \pm SD of three independent experiments. A one-way ANOVA test was performed followed by Bonferroni's multiple comparisons. ***, $P < 0.001$. *n*, number of cells. EABR, ESCRT and ALIX-binding region.

increased ciliation induced by CEP55 knockdown in the presence of serum would be rescued by ectopically expressed GFP-Aurora A proteins (Fig. 5, H–J). These data further suggested that CEP55 regulates cilia disassembly by affecting the protein level of Aurora A.

The chaperonin CCT complex is required for cilia disassembly by stabilizing Aurora A, and CEP55 promotes Aurora A binding to the chaperonin CCT complex

To figure out the possible mechanism by which CEP55 regulates the stability of Aurora A, we performed mass spectrometry during cilia disassembly in HEK293T cells (Fig. S6, A and B) and uncovered several proteins binding CEP55 or Aurora A. Based on these results from mass spectrometry, we established a group of proteins, which are identified both in anti-CEP55 and anti-Aurora A immunoprecipitants, but not in IgG immunoprecipitants (Fig. 6 A). Interestingly, among the top-20 candidates, five proteins are subunits of the CCT (chaperonin-containing TCP1) chaperonin complex, including CCT5, CCT1, CCT8, CCT7, and CCT3. As eukaryotic group II chaperonins, CCT complex is composed of eight arranged homologous subunits (CCT1–CCT8; Frydman et al., 1992; Gao et al., 1992; Ditzel et al., 1998). This complex mediates the folding of their substrate proteins in an ATP-dependent manner, which is required for protein stability and cellular function (Kubota et al., 1995; Spiess et al., 2004). Given that CCT5 has the highest peptide coverage in the CCT complex both in anti-CEP55 and anti-Aurora A immunoprecipitants (Fig. 6 A), we next confirmed whether CCT5 interacts with CEP55 and Aurora A during cilia disassembly. The data showed that both CEP55 and Aurora A were indeed present in anti-CCT5 immunoprecipitants, and vice versa (Fig. 6 B). Meanwhile, CCT1, which ranked only second to CCT5 in these five CCT candidates, was also shown to bind to CEP55 and Aurora A (Fig. 6 B). However, CP110, a well-known ciliogenesis suppressor, did not show any detectable association with these immunoprecipitants (Fig. 6 B). This data indicated that chaperonin CCT complex interacts with CEP55 and Aurora A during cilia disassembly.

Furthermore, we examined the effect of CCT depletion on Aurora A stability. It is well accepted that CCT components within the chaperonin CCT complex are codependent and each depletion will lead to codepletion of other CCT proteins (Freund et al., 2014). The data showed that knockdown any of CCT subunits (CCT1, CCT2, CCT3, CCT4, CCT5, or CCT8) markedly reduced protein levels of Aurora A and slightly decreased in

CEP55 (Fig. 6 C), suggesting that Aurora A is likely to be a potential CCT substrate. A previous study described that most CCT proteins are located at the centrosome, except for CCT2 (Seo et al., 2010). We confirmed the cellular localization of CCT complex with immunofluorescence microscopy (Fig. S6, C–F). Intriguingly, depletion of CEP55 did not affect the localization of CCT proteins (Fig. S6, C–F). It is possible that CEP55 functions as a chaperonin-like protein, interacting with the CCT complex to protect the stability of Aurora A. We further explored the role for the CCT complex in cilia disassembly and found that depletion of CCT1, CCT2, CCT5, or CCT8 individually was also strongly resistant to serum-induced cilia disassembly (Fig. 6 D). Meanwhile, we found that depletion of CCT5 promotes cilia formation in the presence of serum. The increased percentage of ciliated cells induced by CCT5 knockdown was rescued by ectopically expressed GFP-Aurora A proteins (Fig. 6, E and F). These results suggested that the CCT complex acts as a chaperonin of Aurora A protein to regulate cilia disassembly.

Our above data showed that CEP55 regulates cilia disassembly by stabilizing the protein level of Aurora A. Meanwhile, CEP55, Aurora A, and CCT5 form a complex during cilia disassembly. We next analyzed whether CEP55 facilitates the interaction between the chaperonin CCT complex and Aurora A by performing an HA-Aurora A pull-down assay in vitro. Our data showed that the full length of CEP55 obviously increases the coprecipitation of CCT5 with Aurora A (Fig. 6 G). However, 1–355 truncation, which could not bind to Aurora A, failed to promote the interaction between the chaperonin CCT complex and Aurora A (Fig. 6 G). Thus, these data indicated that CEP55 promotes Aurora A binding to the chaperonin CCT complex and subsequently stabilizes the protein level of Aurora A.

Discussion

Primary cilia undergo dynamic assembly and disassembly (Kim and Dynlacht, 2013; Liang et al., 2016; Sánchez and Dynlacht, 2016). Disruption of this balance results in aberrant ciliogenesis, which underlies a group of diseases termed ciliopathies. Here, we established a critical role of cilia disassembly in ciliopathy. Additionally, our study revealed an important molecular mechanism for the protein stability of Aurora A. Thus far, a great deal of proteins has been reported to activate Aurora A kinase during cilia disassembly (Liang et al., 2016), such as HEF-1 (Pugacheva et al., 2007), calmodulin (Plotnikova et al., 2012), Pitchfork (Kinzel et al., 2010), and the Dvl2–Plk1 complex (Lee

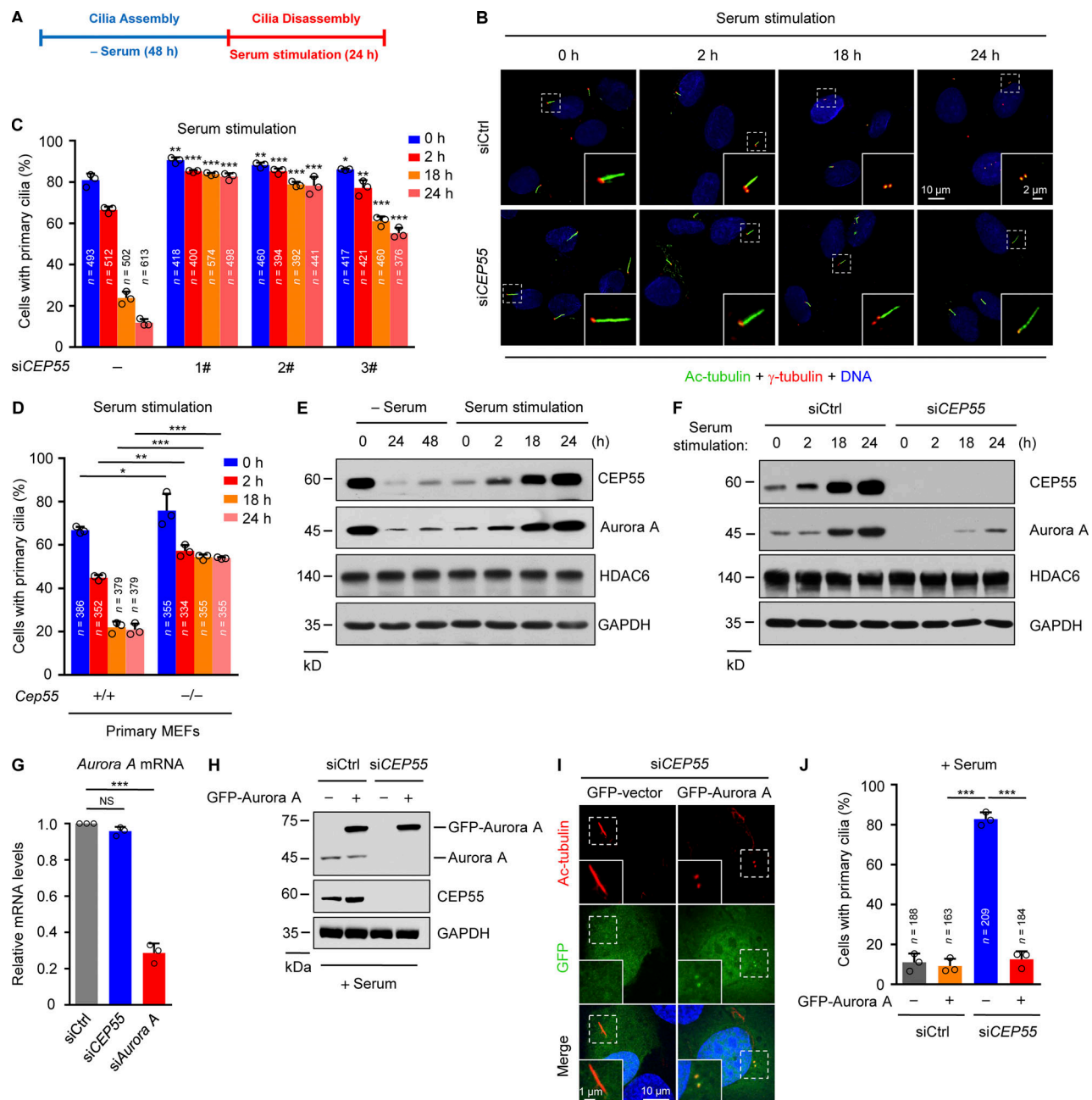


Figure 5. CEP55 promotes cilia disassembly by regulating Aurora A stability. (A) Schematic illustration of experimental strategy used for the cilia assembly and disassembly experiments. (B) RPE-1 cells were transfected with control or CEP55 siRNA and serum starved for 48 h. The ciliated RPE-1 cells were then stimulated with serum for the indicated times and stained with Ac-tubulin (green), γ -tubulin (red), and DNA (blue). Insets show zoomed-in views of the boxed regions. Scale bars, 10 μ m (main image) and 2 μ m (magnified region). (C) Quantification of the percentage of ciliated cells in B with three individual siRNAs against CEP55. Ciliation in siCEP55 groups are compared with their respective time-point controls in siControl group. Data are presented as means \pm SD of three independent experiments. A two-way ANOVA test was performed followed by Dunnett's multiple comparisons. *, $P < 0.05$; **, $P < 0.01$; ***, $P < 0.001$. n , number of cells. (D) Quantification of the percentage of ciliated cells. *Cep55*^{+/+} and *Cep55*^{-/-} primary MEFs were serum starved for 48 h and then stimulated with serum for the indicated times. Data are presented as means \pm SD of three independent experiments. A two-way ANOVA test was performed. *, $P < 0.05$; **, $P < 0.01$; ***, $P < 0.001$. n , number of cells. (E) RPE-1 cells were serum starved (- Serum) and then stimulated with serum (serum stimulation) for the indicated times. The endogenous expressions of CEP55, Aurora A, HDAC6, and GAPDH were determined by immunoblotting with respective antibodies. (F) RPE-1 cells were transfected with control or CEP55 siRNA and serum starved for 48 h. Then, the cells were stimulated with serum for the indicated times. The treated cells were subjected to immunoblotting with the indicated antibodies. (G) mRNA expression levels of *Aurora A* by qRT-PCR were determined from RPE-1 cells transfected with control, CEP55, or *Aurora A* siRNA. Data are means \pm SD of three independent experiments. A one-way ANOVA test was performed followed by Dunnett's multiple comparisons. ***, $P < 0.001$. (H-I) Ciliation in RPE-1 cells induced by CEP55 knockdown were rescued by expressing GFP-Aurora A. GFP-vector (-) or GFP-Aurora A plasmids were transfected in RPE-1 cells after 24 h of siRNA transfection. 24 h later, cell lysates were detected with the indicated antibodies (H) or were stained with Ac-tubulin (red) and DNA (blue; I). Scale bars, 10 μ m (main image) and 1 μ m (magnified region). (J) Quantification of the ciliation in GFP-positive cells in I. Data are presented as means \pm SD of three independent experiments. A two-way ANOVA test was performed followed by Bonferroni's multiple comparisons. ***, $P < 0.001$. n , number of cells.

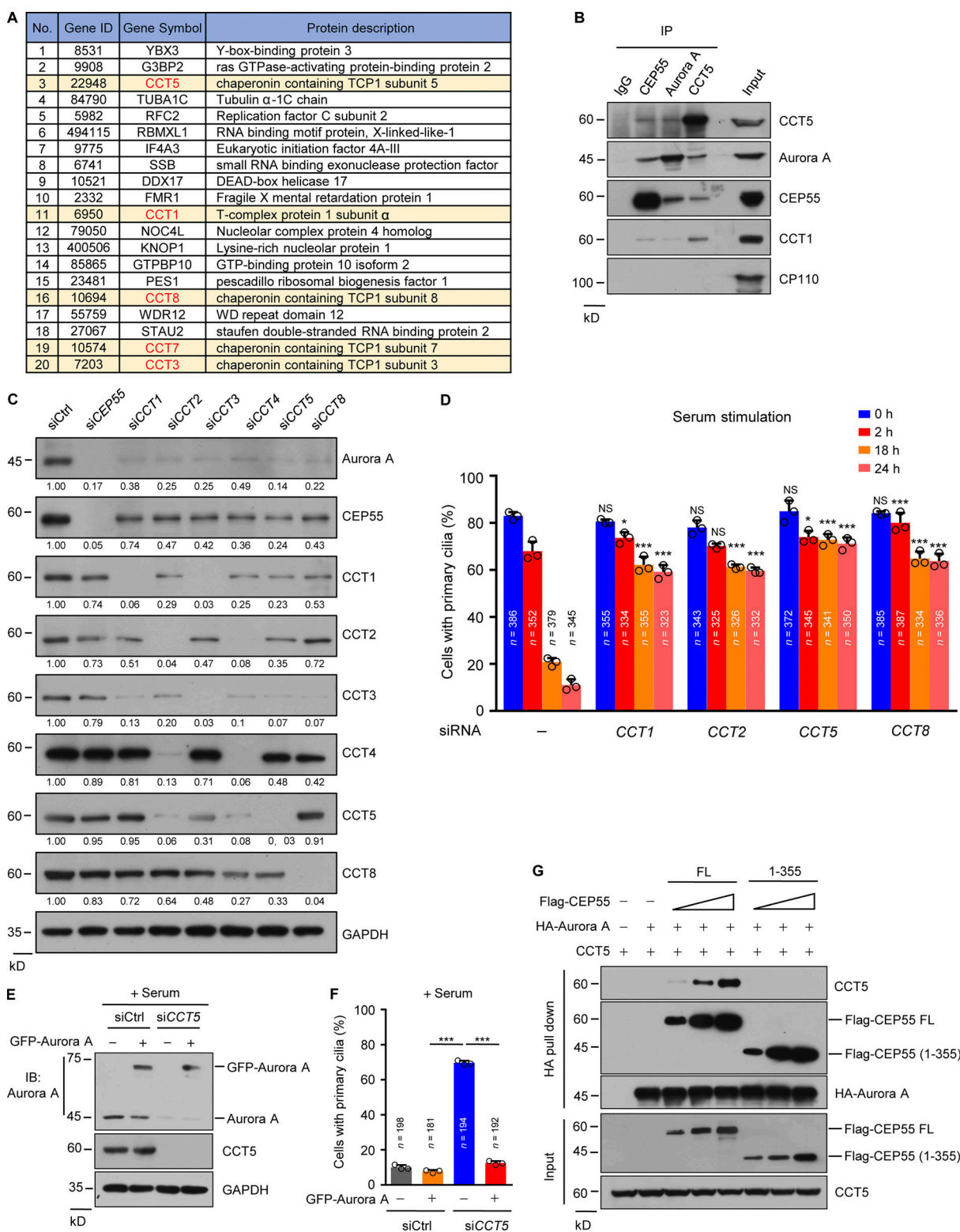


Figure 6. The chaperonin CCT complex is required for cilia disassembly by stabilizing Aurora A, and CEP55 promotes Aurora A binding to the chaperonin CCT complex. (A) HEK293T cells were serum starved for 48 h and then stimulated with serum for 18 h. Endogenous proteins immunoprecipitated with anti-CEP55 or anti-Aurora A antibody from these cells lysates were analyzed by liquid chromatography-tandem mass spectrometry. A list of top-20 proteins identified both in anti-CEP55 and anti-Aurora A immunoprecipitants were shown. (B) HEK293T cell lysates during cilia disassembly were immunoprecipitated with anti-CEP55, anti-Aurora A, anti-CCT5 antibody or normal rabbit IgG, and then the immunoprecipitants were analyzed by immunoblotting with the indicated antibodies. (C) RPE-1 cells were transfected with the indicated siRNAs individually, and cell lysates were detected with the indicated antibodies. The amounts of Aurora A, CEP55, and CCT proteins were quantified in ImageJ software and then normalized to respective GAPDH levels, which is shown at the bottom of each immunoblot. (D) RPE-1 cells were transfected with control, CCT1, CCT2, CCT5, or CCT8 siRNAs and serum starved for 48 h. Next,

ciliated RPE-1 cells were stimulated with serum for the indicated times and then quantified. Ciliation in the siCCT1, siCCT2, siCCT5, or siCCT8 group is compared with their respective time-point controls in the siControl group. Data are presented as means \pm SD of three independent experiments. A two-way ANOVA test was performed followed by Dunnett's multiple comparisons. *, $P < 0.05$; ***, $P < 0.001$. *n*, number of cells. **(E and F)** Increased ciliation in RPE-1 cells induced by CCT5 knockdown were rescued by expressing GFP-Aurora A. GFP-vector (–) or GFP-Aurora A plasmids were transfected in RPE-1 cells after 24 h of siRNA transfection. 24 h later, cell lysates were detected with the indicated antibodies (E). IB, immunoblotting. **(F)** Quantification of the ciliation in GFP-positive cells in E. Data are presented as means \pm SD of three independent experiments. A two-way ANOVA test was performed followed by Bonferroni's multiple comparisons. ***, $P < 0.001$. *n*, number of cells. **(G)** CCT5 binds to Aurora A in the presence of CEP55 in vitro. Increasing amounts of full-length (FL) or 1–355 truncation of Flag-CEP55 proteins were purified from sonicated HEK293T cell lysates by anti-Flag M2 affinity gel, eluted with 3 \times Flag peptide, and then respectively incubated with HA-Aurora A-bound Agarose (pulled down from sonicated HEK293T cell lysates by anti-HA Agarose antibody). HA-vector-bound Agarose was incubated with eluted Flag-vector sample as control (– indicates the corresponding vector). An equal amount of translated CCT5 protein was added to all groups. Proteins retained on anti-HA Agarose were then analyzed by immunoblotting.

et al., 2012). Notably, protein levels of Aurora A are highly oscillatory during the cilia cycle. Protein levels of Aurora A were reduced along with cilia assembly, whereas the levels were restored and up-regulated during cilia disassembly. Similarly, endogenous CEP55 protein levels are dynamically changed, mirroring changes in Aurora A during the cilia cycle. Our study demonstrated that CEP55 stabilizes the protein level of Aurora A through mediating the interaction between Aurora A and CCT chaperonins, which probably functions upstream of HDAC6. Previous studies reported that the main function of CCT chaperonins is to fold the newly synthesized proteins to their native states (Kubota et al., 1995; Spiess et al., 2004). Our study demonstrates that CCT chaperonins interact with and stabilize Aurora A during cilia disassembly, possibly through folding the newly synthesized Aurora A proteins.

It has been reported that aberrant elongated cilia commonly result from defects in retrograde transport or cilia disassembly. Generally, retrograde transport proteins, for example dynein components (Palmer et al., 2011; Avasthi and Marshall, 2012), were reported as the negative modulators of cilia length only under cilia assembly (namely, in the absence of serum). In contrast, silencing of the proteins mediating cilia disassembly not only increases cilia length but also facilitates cilia formation, even in the presence of serum, such as Aurora A (Pugacheva et al., 2007) and Nek2 (Kim et al., 2015). Our results showed that depletion of CEP55 promoted both the elongation and formation of cilia in RPE-1 and primary MEFs. Meanwhile, in agreement with cilia disassembly regulators, overexpression of exogenous CEP55 led to the disappearance of cilia in RPE-1 cells (Inoko et al., 2012; Spalluto et al., 2012). Thus, we suggested that Cep55-deficient mice induced an abnormal elongation of cilia, likely through impaired cilia disassembly process.

Note that the ability to form a cilium for individual cells is strictly determined by their lineage during embryonic development (Bangs et al., 2015), even though they share adjacent locations in the same tissue. Thus, overall, the cells are in two different states, ciliated or nonciliated. When disassembly components are disrupted, the cilium on ciliated cells could display longer. However, nonciliated cells still could not form a cilium due to the shortage of assembly machines (Bangs et al., 2015). Therefore, Cep55-null mice show increased ciliary length in tissues but an unaltered percentage of ciliated cells.

In particular, the loss of cilia on CPECs causes abnormal cerebrospinal fluid circulation (Banizs et al., 2005; Vogel et al., 2012) and is generally considered the primary mechanism for

neonatal hydrocephalus and mortality in MKS (Banizs et al., 2005; Spassky et al., 2005; Tissir et al., 2010; Vogel et al., 2012). In this study, we have shown that Cep55-deficient mice exhibit elongated CPEC cilia and yet also have obvious hydrocephalus and postnatal death. Thus, we have provided some evidence to suggest that deregulated cilia dynamics are also a kind of cilia abnormality, which could be another underlying cause of ciliopathy. However, how abnormal ciliation in Cep55-deficient mice contributes to these MKS phenotypes remains to be addressed in our future study.

Consistent with our data that CEP55 regulates cilia disassembly in vitro, we found that depletion of Cep55 in mice causes abnormally elongated cilia in brain, kidney, and MEFs. Meanwhile, the cell cycle of primary MEFs is also arrested in Cep55-deficient mice. Therefore, it is possible that both abnormal cilia formation and defective proliferation contribute to aberrant brain development in Cep55-deficient mice. Mice homozygous for the Aurora A-null allele display embryonic mortality before implantation due to early embryonic growth arrest and impaired mitosis (Lu et al., 2008; Cowley et al., 2009). Moreover, heterozygous Pitchfork-null embryos generated by tetraploid complementation mice display embryonic lethality with heart failure and a node cilia duplication phenotype (Kinzel et al., 2010). Unlike those two, Cep55-deficient mice are characterized by perinatal death. Meanwhile, along with a homozygous nonsense mutation (c.256C>T; Bondeson et al., 2017), a new homozygous frameshift variant (c.514dup) in CEP55 was identified with a severe syndromic fetal lethal disorder (Rawlins et al., 2019). All of the above provide a novel view into cilia disassembly during embryonic development and ciliopathy. Thus, identification of this new role of CEP55 enabled molecular genetic testing to allow accurate perinatal diagnosis and potential treatment of ciliopathies.

Materials and methods

Mice

Cep55^{loxP/loxP} mice were generated by Cas9-CRISPR-mediated genome editing (Nanjing Biomedical Research Institute of Nanjing University). Briefly, the 5' sgRNA sequence TAGAGG TGATGGGGTCATGAGGG and 3' sequence GGAATGAGCACT TTGAGAAAGGG were inserted into the gRNA cloning vector. Both donor vectors were 1.9-kbp double-stranded DNA containing homologous arms, loxP sites, and restriction sites. Then, two sgRNAs, Cas9 mRNA, and donor vectors were coinjected

into fertilized eggs and transferred into foster mothers. Positive F0 mice genotyped by PCR were mated with wild-type C57BL/6 mice, and positive F1 mice were then selected to obtain *Cep55*-floxed mice. Subsequently, *Cep55^{loxP/loxP}* mice were crossed with EIIa-Cre mice (stock no. 003724; Jackson Laboratory), and deletion of the floxed region created a frameshift, resulting in a null allele (*Cep55^{-/-}*) mice. The pups were genotyped by PCR followed by sequence analysis using primers (mouse *Cep55*-F: 5'-TGTCTGGTAAGGATCTTCAAGCTG-3'; mouse *Cep55*-R: 5'-TGGAAGTTAGCTTGGGCTACG-3'). Animals were housed in a pathogen-free facility under a 12-h light cycle. All embryos used for this study were obtained from natural matings of virgin females 8–10 wk old. Noon on the day of the discovery of a vaginal plug was considered to be E0.5. All animal experiments were performed with the approval of the institutional animal care and use committee of our institution.

Cell culture

Human hTERT RPE-1 (RPE-1) cells were kindly provided by Xueliang Zhu (Shanghai Institute of Biochemistry and Cell Biology, Shanghai, China) and cultured in DMEM/F-12 (1:1) supplemented with 10% FBS, 0.01 mg/ml hygromycin B, and 1% penicillin/streptomycin. For cilia formation, RPE-1 cells were starved in Opti-MEM reduced serum media (Thermo Fisher Scientific) for 48 h. *Cep55^{+/+}* and *Cep55^{-/-}* primary MEFs were derived from E13.5 mouse embryos. Briefly, mouse embryos were dissected from the placenta and their organs, head, limbs, and tail removed. Fibroblasts were isolated from minced and trypsinized tissue (37°C, 30 min). Primary MEFs were grown in DMEM supplemented with 15% FBS and used for analysis at passage 3 or lower. For Smo localization analysis, primary MEFs were starved in Opti-MEM for 48 h and then treated with 500 nM SAG (566660; Sigma-Aldrich) for 6 h. Human embryonic kidney cells (HEK293T) were maintained in DMEM supplemented with 10% FBS.

Electroporation

MEF Nucleofector Kits (Lonza) were used for transfection of MEFs, according to the manufacturer's guidelines (VPD-1005). siRNAs were used to transfect $3\text{--}4 \times 10^6$ cells per 6-cm dish. After electroporation, cells were collected 48 h after transfection.

Cloning and plasmids

Plasmids expressing recombinant Flag-CEP55 were kindly gifted by Kerstin Kutsche and then reconstructed into the p-mCherry-C1-vector. mCherry-CEP55-WT, mCherry-CEP55-3SA, full-length and truncations of Flag-CEP55 (residues 1–217, 217–464, 217–355, 355–464, and 1–355), mCherry-CEP55 siRNA-resistant plasmids, and mCherry-CEP55-C256T mutants were generated by PCR-based site-directed mutagenesis. cDNA encoding Aurora A was subcloned into pEGFP-C1-vector and pXJ40-HA-vector for expression in mammalian cells. All constructs were verified by DNA sequencing. Plasmid transfection into RPE-1 cells was performed using Lipofectamine LTX Reagent (Thermo Fisher Scientific) according to the manufacturer's instructions.

RNAi

Synthetic siRNA oligonucleotides were obtained from Thermo Fisher Scientific. Transfection of siRNAs using RNAiMAX (Thermo Fisher Scientific) was performed according to the manufacturer's instructions. siRNA#1 was used in all *CEP55* RNAi experiments in this study, unless otherwise indicated. The sequences of siRNAs (Thermo Fisher Scientific) are as follows: control siRNA: 5'-UUCUCCGAA CGUGUCACGUAA-3'; *CEP55* siRNA (#1): 5'-GGAAGAUGAUAGGCAUAAA-3'; *CEP55* siRNA (#2): 5'-ACGAAUUGCUGAACUUGAAAGCAAA-3'; *CEP55* siRNA (#3): 5'-GAGGGAGCAGGUGUUGAAAGCCUUA-3'; *Aurora A* siRNA: 5'-GGGUAAAGGAAAGUUUGGUAUGUU-3'; *Ift20* siRNA (mouse): 5'-AGAAAGGUAUCG GGUUGAAUUAUGAA-3'; *CCT1* siRNA: 5'-GCAAGAUACUUCUUGUUAUU-3'; *CCT2* siRNA: 5'-GUUGAC AAUCCAGCAGCUA-3'; *CCT3* siRNA: 5'-GCCAAGUCCAUGAUCGAA AUU-3'; *CCT4* siRNA: 5'-GAACUGAGUGACAGAGAAAUU-3'; *CCT5* siRNA: 5'-CAAGUCUCAGGAUGAUGAA-3'; *CCT8* siRNA: 5'-CUU CGUACCUCCAUAUAUGA-3'.

Immunofluorescence microscopy

For tissue immunofluorescence, brains and kidneys were fixed in 4% PFA at 4°C overnight or for 2 h and then embedded in OCT compound (Sakura). Frozen sections were cut at 10 μ m.

RPE-1 cells transfected with plasmids, primary MEFs, and HEK293T cells were fixed in 4% PFA for 10 min at 37°C and –20°C methanol for 2 min. For detection of primary cilia, cells were placed on ice for 10 min before fixation and stained with anti-acetylated (Ac)-tubulin antibody. To visualize centrosome proteins in RPE-1 cells, cells were fixed and permeabilized in –20°C methanol for 5–10 min. To label cells in S phase, cultured cells were treated with 10 μ M EdU (Thermo Fisher Scientific) for 1 h before fixation. EdU staining was then performed using the Click-iT EdU imaging kit (Thermo Fisher Scientific) according to the manufacturer's instructions.

Tissue sections were and cells were blocked with 3% BSA and 1% normal goat serum in 0.1% Triton X-100/PBS before incubation with primary antibodies. Secondary antibodies used were Alexa Fluor 488–, 546–, 647–conjugated goat anti-mouse or anti-rabbit IgG (Thermo Fisher Scientific). DNA was stained with Hoechst 33342 (1:1,000, H3570; Thermo Fisher Scientific).

Images were acquired at room temperature with a 60 \times /1.42 oil objective (Fig. 2, C, E, and L; and Fig. 3, Fig. 4, Fig. 5, Fig. S1, Fig. S3, Fig. S4, and Fig. S6) or with a 40 \times /1.42 oil objective (Fig. 2 A) on DeltaVision Image Restoration Microscope (with an sCMOS edge5.5 camera), with a 10 \times /0.45 objective (Figs. 2 J, S2 A, and S5 A) or a 63 \times /1.40 oil objective on Zeiss LSM 880 (Fig. 1 J), or a 63 \times /1.40 oil objective on Zeiss LSM 880 with Airyscan (Fig. 1 D). All acquisition settings were kept constant for experimental and control groups in the same experiment. The representative images acquired by the DeltaVision system were processed by iterative constrained deconvolution (SoftWoRx; Applied Precision Instruments). All raw images were analyzed with Volocity 6.0 software (Perkin Elmer). Cilium length was measured from the tip of cilia to the base.

Immunohistochemistry and histology

Tissues were fixed in 4% PFA overnight, embedded in paraffin following standard procedures, and then stained with hematoxylin

and eosin (Fig. 1, B, C, and I; and Fig. S1, E and F). Images were captured using a NanoZoomer Digital Pathology system (Hamamatsu Photonics).

Scanning electron microscopy

For scanning electron microscopy, samples were fixed overnight at 4°C in 2.5% glutaraldehyde and 2% PFA in 0.1 M phosphate buffer (pH 7.4). After serial dehydration in increasing ethanol concentrations, samples were dried at critical point and coated with gold using standard procedures. Observations were made in a Quanta FEG 250 (Thermo Fisher Scientific).

MRI

Cep55^{+/+} and *Cep55*^{-/-} littermates at E18.5 were embedded in 3% agarose and taken out before MRI scanning. MRI was performed by a small-animal MRI Facility (PharmaScan 70/16 US; Bruker) with the Paravision 6.0.1 software platform. Mice were positioned in a 72-mm radio frequency coil equipped with a rat head surface coil. The scan protocol for axial images was T2_TurboRare with the following parameters: TR/TE (ratio of repetition time/echo time): 4,500/120 ms, FOV (field of view) 20 × 20 cm, image size 256 × 256, slice thickness 0.7 mm, 25 averages. The scan protocol for sagittal images was T2_TurboRare with the following parameters: TR/TE: 4,500/100 ms, FOV 20 × 20 cm, image size 256 × 256, slice thickness 0.7 mm, 20 averages.

Immunoblotting analysis

Cells were lysed with lysis buffer (20 mM Tris-HCl, pH 7.5, 150 mM NaCl, 10 mM EDTA, 1% Triton X-100, and 1% deoxycholate) containing complete protease inhibitor cocktail (04693132001; Roche). Cell lysates were separated by SDS-PAGE and analyzed by Western blotting with the indicated antibodies. Proteins were visualized by chemiluminescence according to the manufacturer's instructions.

Flow cytometry analysis

For analyzing cell cycle profiles, primary MEFs were fixed with 70% ice-cold ethanol, washed with PBS twice, and incubated in 50 mg/ml propidium iodide and 50 mg/ml RNase A for 30 min. The data were acquired by BD FACSaria II and analyzed by using the ModFit software.

RNA isolation and quantitative real-time PCR (qRT-PCR)

Total RNA was extracted with TRIzol reagent (93289; Sigma-Aldrich). To determine relative mRNA levels, qRT-PCR was performed using SYBR Premix Ex Taq II (DRR081A; Takara), and gene expression was normalized to that of GAPDH (control housekeeping gene). qRT-PCR assays were run on an ABI StepOnePlus system (Thermo Fisher Scientific) according to the manufacturer's protocol. Data were analyzed with StepOnePlus software. The primers used to amplify the target genes are as follows: *CEP55*-F: 5'-AGTAAGTGGGATCGAAGCCT-3'; *CEP55*-R: 5'-CTCAAGGACTCGAATTTCTCCA-3'; *Aurora A*-F: 5'-GAGGTC CAAAACGTGTTCTCG-3'; *Aurora A*-R: 5'-ACAGGATGAGGTACACTG GTTG-3'; *GAPDH*-F: 5'-GGAGCGAGATCCCTCCAAAT-3'; *GAPDH*-R: 5'-GGCTGTTGTCATACTTCTCATGG-3'.

Immunoprecipitation and mass spectrometry

For coimmunoprecipitation (IP) experiments, HEK293T cells were transfected with the indicated plasmids. At 24 h after transfection, cells were washed twice with PBS and lysed in IP lysis buffer (50 mM Tris-HCl, pH 7.5, 1% NP-40, 150 mM NaCl, 0.5 mM EGTA, 0.5 mM EDTA, 1 mM DTT, 1.5 mM MgCl₂, and 1 mM PMSF) containing complete protease inhibitor and phosphoSTOP (4906837001; Roche). The lysates were centrifuged at 12,000 g at 4°C for 15 min. Supernatants were incubated with anti-Flag M2 Affinity Gel (A2220; Sigma-Aldrich) for 4 h at 4°C. The immunoprecipitants were washed six times with the same IP lysis buffer. The immunoprecipitated proteins were removed from M2 Affinity Gel by boiling for 10 min in SDS-sample buffer and immunoblotted with indicated antibody.

For immunoprecipitation experiments, HEK293T cells or primary MEFs were collected in IP lysis buffer. Extracts were cleared by subsequent centrifugations. Supernatants were incubated with rabbit anti-CEP55, anti-Aurora A, anti-CCT5 antibody, or normal rabbit IgG (sc-2027; Santa Cruz Biotechnology) with rotation overnight at 4°C. Then, Protein A Sepharose (17-1279-01; GE) was added, and samples were rotated for 2 h at 4°C. The immunoprecipitants were washed and boiled and then analyzed by immunoblotting.

For the HA-Aurora A pull-down assay in vitro, HEK293T cells were transfected with HA-vector or HA-Aurora A plasmids, respectively, and lysed with NP-40 buffer (AR0107; BOSTER) containing complete protease inhibitor and phosphoSTOP. Then, the HA-Aurora A proteins were purified from sonicated lysates by anti-HA Agarose antibody (A2095; Sigma-Aldrich). To obtain purified CEP55 proteins, full-length or 1-355 truncation of Flag-CEP55 plasmids were transfected in HEK293T cells. Then cell lysates were immunoprecipitated by anti-Flag M2 Affinity Gel, and immunoprecipitants were eluted with 3×Flag peptide (F4799; Sigma-Aldrich) in elution buffer (50 mM Tris-HCl, pH 7.4, and 150 mM NaCl) for 2 h. To get CCT5 proteins, CCT5 plasmids were translated in vitro with a TNT T7 Quick Coupled Transcription/Translation Systems (LI170; Promega). Then, the eluted full-length or 1-355 truncation of CEP55 proteins were incubated with equal amount of HA-Aurora A-bound agarose and translated CCT5 proteins overnight at 4°C. The final immunoprecipitants were washed and detected by immunoblotting.

For mass spectrometry analysis, gels were stained with Bio-Safe Coomassie (Bio-Rad). After Coomassie staining, gels of panels were respectively excised and digested in-gel with trypsin. Mass spectrometry analysis was performed on an LTQ-Orbitrap Velos mass spectrometer (Thermo Fisher Scientific).

Antibodies and reagents

Antibodies used in this study included mouse anti-GT335 (1:200, AG-20B-0020B-C100; Adipogen), mouse anti-Actubulin (1:500, T6793; Sigma-Aldrich), rabbit anti-γ-tubulin (1:200, T5192; Sigma-Aldrich), rabbit anti-CEP55 (Western blot [WB], 1:1,000, 81693; Cell Signaling Technologies; immunofluorescence [IF], 1:200, ab170414; Abcam), mouse anti-CEP55 (WB, 1:1,000, H00055165-A01; Abnova), mouse anti-Smo (1:200, sc23929; Santa Cruz Biotechnology), rabbit anti-IFT20 (WB, 1:1,000,

13615-1-AP; Proteintech), rabbit anti-mCherry (1:1,000, ab167453; Abcam), rabbit anti-Aurora A (WB, 1:1,000; IF, 1:200; 14475; Cell Signaling Technologies), mouse anti-Aurora A (WB, 1:1,000, 610938; BD Biosciences), rabbit anti-HDAC6 (WB, 1:1,000, 7612; Cell Signaling Technologies), rabbit anti-phospho-Aurora A (T288; IF, 1:200, 3079; Cell Signaling Technologies), mouse anti-Flag (WB, 1:1,000; IF, 1:500; F3165; Sigma-Aldrich), anti-DDDDK-tag pAb-HRP-Direct (PM020-7; MBL), mouse anti-centrin2 (1:400, 04-1624; Millipore), rabbit anti-ARL13B (1:500, 17711-1-AP; Proteintech), rabbit anti-CEP164 (1:600, 45330002; Novus), rabbit anti-PCM1 (1:500, 5213; Cell Signaling Technologies), rabbit anti-CCT1 (1:5,000, 10320-1-AP; Proteintech), rabbit anti-CCT2 (1:5,000, 24896-1-AP; Proteintech), rabbit anti-CCT3 (1:5,000, 10571-1-AP; Proteintech), rabbit anti-CCT4 (1:5,000, 21524-1-AP; Proteintech), rabbit anti-CCT5 (1:5,000, 11603-1-AP; Proteintech), rabbit anti-CCT8 (1:5,000, 12263-1-AP; Proteintech), mouse anti-HA (1:1,000, sc-7392; Santa Cruz), and rabbit anti- α -tubulin (1:1,000, PM054; MBL). Polyclonal antibodies against GAPDH were prepared in our laboratory.

Statistics

Statistical calculations were performed with SPSS software. We tested the normality of all data using Shapiro-Wilk tests in SPSS. A P value > 0.05 means the null hypothesis (that the distribution is normal) is accepted. A P value < 0.05 means that the null hypothesis is rejected and the distribution is not normal. Statistical comparisons between two groups conformed to a normal distribution were performed by unpaired two-tailed t tests. Multiple comparisons were performed by using one-way or two-way ANOVA followed by Bonferroni's or Dunnett's multiple comparisons, as noted in the figure legends. The exact sample sizes (n) used to calculate statistics are provided in the figure legends. For all tests, differences were considered statistically significant if P values were < 0.05 (as indicated with *, $P < 0.05$; **, $P < 0.01$; and ***, $P < 0.001$). No statistical methods were used to predetermine sample size. The experiments were not randomized. No samples were excluded. The investigators were blinded for assessment of all staining assays.

Data availability

The data that support the findings of this study are available from the corresponding author upon reasonable request.

Online supplemental material

Fig. S1 shows that targeted disruption of the *Cep55* gene in mice and phenotypes of the face and limb from *Cep55*^{+/+} and *Cep55*^{-/-} mice. **Fig. S2** illustrates that *Cep55* deficiency does not affect the mitotic progression in cerebral cortex. **Fig. S3** shows that CEP55 is dispensable for the centrosome integrity and its localization in different cell cycle stages. **Fig. S4** shows that CEP55 interacts with Aurora A and localizes at the centrosome. **Fig. S5** illustrates that *Cep55* deficiency inhibits cilia disassembly and the stability of Aurora A protein in primary MEFs. **Fig. S6** illustrates cilia assembly and disassembly in HEK293T cells and the localization of CCT proteins in CEP55-depleted cells. Table S1 lists genotype distributions of offspring of *Cep55* heterozygous mice intercrossed at different ages.

Acknowledgments

We would like to thank Professor Xue-liang Zhu (Chinese Academy of Sciences, Institute of Biochemistry and Cell Biology, Shanghai, China), Kerstin Kutsche (University Medical Center Hamburg-Eppendorf, Hamburg, Germany), and Jeremy F. Reiter (University of California, San Francisco, San Francisco, CA) for providing cells, plasmids, antibodies, and technical support.

This work was funded by the National Basic Research Program of China (grants 2014CB910603 and 2013CB910302), the National Natural Science Foundation of China (grants 81521064 and 81790252), the National Key Research and Development Program (grants 2017YFC1601100, 2017YFC1601101, 2017YFC1601102, and 2017YFC1601104), and the National Major Science and Technology Projects of China ("Significant New Drugs Development").

The authors declare no competing financial interests.

Author contributions: H-Y. Li, T. Zhou, and M. Wu supervised the project; Y-C. Zhang and Y-F. Bai designed and carried out most of the experiments; J-F. Yuan, S. Li, Y-L. Xu, P-Y. Li, Q-Y. Han, and X-L. Shen provided reagents and suggestions; Z-Q. Song, H-B. Hu, X-X. Jian, and H-Q. Tu analyzed the data; N. Wang and A-L. Li carried out the statistics; and Y-C. Zhang, Y-F. Bai, H-Y. Li, and X-M. Zhang wrote the paper. All authors discussed the results and commented on the manuscript.

Submitted: 24 March 2020

Revised: 24 August 2020

Accepted: 23 November 2020

References

- Aguilar, A., A. Meunier, L. Strehl, J. Martinovic, M. Bonniere, T. Attie-Bitach, F. Encha-Razavi, and N. Spassky. 2012. Analysis of human samples reveals impaired SHH-dependent cerebellar development in Joubert syndrome/Meckel syndrome. *Proc. Natl. Acad. Sci. USA*. 109:16951-16956. <https://doi.org/10.1073/pnas.1201408109>
- Ahdab-Barmada, M., and D. Claassen. 1990. A distinctive triad of malformations of the central nervous system in the Meckel-Gruber syndrome. *J. Neuropathol. Exp. Neurol.* 49:610-620. <https://doi.org/10.1097/00005072-199011000-00007>
- Avasthi, P., and W.F. Marshall. 2012. Stages of ciliogenesis and regulation of ciliary length. *Differentiation*. 83:S30-S42. <https://doi.org/10.1016/j.diff.2011.11.015>
- Badano, J.L., N. Mitsuma, P.L. Beales, and N. Katsanis. 2006. The ciliopathies: an emerging class of human genetic disorders. *Annu. Rev. Genomics Hum. Genet.* 7:125-148. <https://doi.org/10.1146/annurev.genom.7.080505.115610>
- Bangs, F.K., N. Schrode, A.K. Hadjantonakis, and K.V. Anderson. 2015. Lineage specificity of primary cilia in the mouse embryo. *Nat. Cell Biol.* 17: 113-122. <https://doi.org/10.1038/ncb3091>
- Banizs, B., M.M. Pike, C.L. Millican, W.B. Ferguson, P. Komlosi, J. Sheetz, P.D. Bell, E.M. Schwiebert, and B.K. Yoder. 2005. Dysfunctional cilia lead to altered endoderm and choroid plexus function, and result in the formation of hydrocephalus. *Development*. 132:5329-5339. <https://doi.org/10.1242/dev.02153>
- Blacque, O.E., and M.R. Leroux. 2006. Bardet-Biedl syndrome: an emerging pathomechanism of intracellular transport. *Cell. Mol. Life Sci.* 63: 2145-2161. <https://doi.org/10.1007/s00018-006-6180-x>
- Blacque, O.E., M.J. Reardon, C. Li, J. McCarthy, M.R. Mahjoub, S.J. Ansley, J.L. Badano, A.K. Mah, P.L. Beales, W.S. Davidson, et al. 2004. Loss of C. elegans BBS-7 and BBS-8 protein function results in cilia defects and compromised intraflagellar transport. *Genes Dev.* 18:1630-1642. <https://doi.org/10.1101/gad.1194004>
- Bondeson, M.L., K. Ericson, S. Gudmundsson, A. Ameur, F. Pontén, J. Westström, C. Frykholm, and M. Wilbe. 2017. A nonsense mutation in CEP55 defines a new locus for a Meckel-like syndrome, an autosomal

- recessive lethal fetal ciliopathy. *Clin. Genet.* 92:510–516. <https://doi.org/10.1111/cge.13012>
- Burtey, S., M. Riera, E. Ribe, P. Pennenkamp, R. Rance, J. Luciani, B. Dworniczak, M.G. Mattei, and M. Fontés. 2008. Centrosome overduplication and mitotic instability in PKD2 transgenic lines. *Cell Biol. Int.* 32: 1193–1198. <https://doi.org/10.1016/j.cellbi.2008.07.021>
- Carlton, J.G., and J. Martin-Serrano. 2007. Parallels between cytokinesis and retroviral budding: a role for the ESCRT machinery. *Science*. 316: 1908–1912. <https://doi.org/10.1126/science.1143422>
- Carlton, J.G., M. Agromayor, and J. Martin-Serrano. 2008. Differential requirements for Alix and ESCRT-III in cytokinesis and HIV-1 release. *Proc. Natl. Acad. Sci. USA*. 105:10541–10546. <https://doi.org/10.1073/pnas.0802008105>
- Cowley, D.O., J.A. Rivera-Pérez, M. Schliekelman, Y.J. He, T.G. Oliver, L. Lu, R. O'Quinn, E.D. Salmon, T. Magnuson, and T. Van Dyke. 2009. Aurora-A kinase is essential for bipolar spindle formation and early development. *Mol. Cell Biol.* 29:1059–1071. <https://doi.org/10.1128/MCB.01062-08>
- Ditzel, L., J. Löwe, D. Stock, K.O. Stetter, H. Huber, R. Huber, and S. Steinbacher. 1998. Crystal structure of the thermosome, the archaeal chaperonin and homolog of CCT. *Cell*. 93:125–138. [https://doi.org/10.1016/S0092-8674\(00\)81152-6](https://doi.org/10.1016/S0092-8674(00)81152-6)
- Fabbro, M., B.B. Zhou, M. Takahashi, B. Sarcevic, P. Lal, M.E. Graham, B.G. Gabrielli, P.J. Robinson, E.A. Nigg, Y. Ono, and K.K. Khanna. 2005. Cdk1/Erk2- and Plk1-dependent phosphorylation of a centrosome protein, Cep55, is required for its recruitment to midbody and cytokinesis. *Dev. Cell*. 9:477–488. <https://doi.org/10.1016/j.devcel.2005.09.003>
- Fliegauf, M., J. Horvath, C. von Schnakenburg, H. Olbrich, D. Müller, J. Thumfart, B. Schermer, G.J. Pazour, H.P. Neumann, H. Zentgraf, et al. 2006. Nephrocystin specifically localizes to the transition zone of renal and respiratory cilia and photoreceptor connecting cilia. *J. Am. Soc. Nephrol.* 17:2424–2433. <https://doi.org/10.1681/ASN.2005121351>
- Follit, J.A., R.A. Tuft, K.E. Fogarty, and G.J. Pazour. 2006. The intraflagellar transport protein IFT20 is associated with the Golgi complex and is required for cilia assembly. *Mol. Biol. Cell*. 17:3781–3792. <https://doi.org/10.1091/mbc.e06-02-0133>
- Frank, V., A.I. den Hollander, N.O. Brückle, M.N. Zonneveld, G. Nürnberg, C. Becker, G. Du Bois, H. Kendziorra, S. Roosing, J. Senderek, et al. 2008. Mutations of the CEP290 gene encoding a centrosomal protein cause Meckel-Gruber syndrome. *Hum. Mutat.* 29:45–52. <https://doi.org/10.1002/humu.20614>
- Freund, A., F.L. Zhong, A.S. Venteicher, Z. Meng, T.D. Veenstra, J. Frydman, and S.E. Artandi. 2014. Proteostatic control of telomerase function through TRiC-mediated folding of TCAB1. *Cell*. 159:1389–1403. <https://doi.org/10.1016/j.cell.2014.10.059>
- Frydman, J., E. Nimmesgern, H. Erdjument-Bromage, J.S. Wall, P. Tempst, and F.U. Hartl. 1992. Function in protein folding of TRiC, a cytosolic ring complex containing TCP-1 and structurally related subunits. *EMBO J.* 11: 4767–4778. <https://doi.org/10.1002/j.1460-2075.1992.tb05582.x>
- Gao, Y., J.O. Thomas, R.L. Chow, G.H. Lee, and N.J. Cowan. 1992. A cytoplasmic chaperonin that catalyzes beta-actin folding. *Cell*. 69: 1043–1050. [https://doi.org/10.1016/0092-8674\(92\)90622-j](https://doi.org/10.1016/0092-8674(92)90622-j)
- Gerdes, J.M., and N. Katsanis. 2008. Ciliary function and Wnt signal modulation. *Curr. Top. Dev. Biol.* 85:175–195. [https://doi.org/10.1016/S0070-2153\(08\)00807-7](https://doi.org/10.1016/S0070-2153(08)00807-7)
- Goetz, S.C., and K.V. Anderson. 2010. The primary cilium: a signalling centre during vertebrate development. *Nat. Rev. Genet.* 11:331–344. <https://doi.org/10.1038/nrg2774>
- Gogusev, J., I. Murakami, M. Doussau, L. Telvi, A. Stojkoski, P. Lesavre, and D. Droz. 2003. Molecular cytogenetic aberrations in autosomal dominant polycystic kidney disease tissue. *J. Am. Soc. Nephrol.* 14:359–366. <https://doi.org/10.1097/01.ASN.0000046963.60910.63>
- Green, R.A., E. Paluch, and K. Oegema. 2012. Cytokinesis in animal cells. *Annu. Rev. Cell Dev. Biol.* 28:29–58. <https://doi.org/10.1146/annurev-cellbio-101011-155718>
- Hartill, V., K. Szymanska, S.M. Sharif, G. Whewey, and C.A. Johnson. 2017. Meckel-Gruber Syndrome: An Update on Diagnosis, Clinical Management, and Research Advances. *Front. Pediatr.* 5:244. <https://doi.org/10.3389/fped.2017.00244>
- Hong, C.J., and B.A. Hamilton. 2016. Zfp423 Regulates Sonic Hedgehog Signaling via Primary Cilium Function. *PLoS Genet.* 12:e1006357. <https://doi.org/10.1371/journal.pgen.1006357>
- Inoko, A., M. Matsuyama, H. Goto, Y. Ohmuro-Matsuyama, Y. Hayashi, M. Enomoto, M. Ibi, T. Urano, S. Yonemura, T. Kiyono, et al. 2012. Trichoplein and Aurora A block aberrant primary cilia assembly in proliferating cells. *J. Cell Biol.* 197(3):391–405. <https://doi.org/10.1083/jcb.201106101>
- Kim, S., and B.D. Dynlacht. 2013. Assembling a primary cilium. *Curr. Opin. Cell Biol.* 25:506–511. <https://doi.org/10.1016/j.ccb.2013.04.011>
- Kim, S., K. Lee, J.H. Choi, N. Ringstad, and B.D. Dynlacht. 2015. Nek2 activation of Kif24 ensures cilium disassembly during the cell cycle. *Nat. Commun.* 6:8087. <https://doi.org/10.1038/ncomms9087>
- Kinzel, D., K. Boldt, E.E. Davis, I. Bartscher, D. Trümbach, B. Diplas, T. Attié-Bitach, W. Wurst, N. Katsanis, M. Ueffing, and H. Lickert. 2010. Pitchfork regulates primary cilia disassembly and left-right asymmetry. *Dev. Cell*. 19:66–77. <https://doi.org/10.1016/j.devcel.2010.06.005>
- Kubota, H., G. Hynes, and K. Willison. 1995. The chaperonin containing t-complex polypeptide 1 (TCP-1). Multisubunit machinery assisting in protein folding and assembly in the eukaryotic cytosol. *Eur. J. Biochem.* 230:3–16. <https://doi.org/10.1111/j.1432-1033.1995.tb20527.x>
- Kyttälä, M., J. Tallila, R. Salonen, O. Kopra, N. Kohlschmidt, P. Paavola-Sakki, L. Peltonen, and M. Kestilä. 2006. MKS1, encoding a component of the flagellar apparatus basal body proteome, is mutated in Meckel syndrome. *Nat. Genet.* 38:155–157. <https://doi.org/10.1038/ng1714>
- Lambacher, N.J., A.L. Bruel, T.J. van Dam, K. Szymanska, G.G. Slaats, S. Kuhns, G.J. McManus, J.E. Kennedy, K. Gaff, K.M. Wu, et al. 2016. TMEM107 recruits ciliopathy proteins to subdomains of the ciliary transition zone and causes Joubert syndrome. *Nat. Cell Biol.* 18:122–131. <https://doi.org/10.1038/ncb3273>
- Lee, H.H., N. Elia, R. Ghirlando, J. Lippincott-Schwartz, and J.H. Hurley. 2008. Midbody targeting of the ESCRT machinery by a noncanonical coiled coil in CEP55. *Science*. 322:576–580. <https://doi.org/10.1126/science.1162042>
- Lee, K.H., Y. Johmura, L.R. Yu, J.E. Park, Y. Gao, J.K. Bang, M. Zhou, T.D. Veenstra, B. Yeon Kim, and K.S. Lee. 2012. Identification of a novel Wnt5a-Ck1ε-Dvl2-Plk1-mediated primary cilia disassembly pathway. *EMBO J.* 31:3104–3117. <https://doi.org/10.1038/emboj.2012.144>
- Liang, Y., D. Meng, B. Zhu, and J. Pan. 2016. Mechanism of ciliary disassembly. *Cell. Mol. Life Sci.* 73:1787–1802. <https://doi.org/10.1007/s00018-016-2148-7>
- Lu, L.Y., J.L. Wood, L. Ye, K. Minter-Dykhouse, T.L. Saunders, X. Yu, and J. Chen. 2008. Aurora A is essential for early embryonic development and tumor suppression. *J. Biol. Chem.* 283:31785–31790. <https://doi.org/10.1074/jbc.M805880200>
- Martinez-Garay, I., A. Rustom, H.H. Gerdes, and K. Kutsche. 2006. The novel centrosomal associated protein CEP55 is present in the spindle midzone and the midbody. *Genomics*. 87:243–253. <https://doi.org/10.1016/j.ygeno.2005.11.006>
- Morita, E., L.A. Colf, M.A. Karren, V. Sandrin, C.K. Rodesch, and W.I. Sundquist. 2010. Human ESCRT-III and VPS4 proteins are required for centrosome and spindle maintenance. *Proc. Natl. Acad. Sci. USA*. 107: 12889–12894. <https://doi.org/10.1073/pnas.1005938107>
- Narita, K., and S. Takeda. 2015. Cilia in the choroid plexus: their roles in hydrocephalus and beyond. *Front. Cell. Neurosci.* 9:39. <https://doi.org/10.3389/fncel.2015.00039>
- Palmer, K.J., L. MacCarthy-Morrogh, N. Smyllie, and D.J. Stephens. 2011. A role for Tctex-1 (DYNLT1) in controlling primary cilium length. *Eur. J. Cell Biol.* 90:865–871. <https://doi.org/10.1016/j.ejcb.2011.05.003>
- Paridaen, J.T., M. Wilsch-Bräuninger, and W.B. Huttner. 2013. Asymmetric inheritance of centrosome-associated primary cilium membrane directs ciliogenesis after cell division. *Cell*. 155:333–344. <https://doi.org/10.1016/j.cell.2013.08.060>
- Plotnikova, O.V., A.S. Nikonova, Y.V. Loskutov, P.Y. Kozyulina, E.N. Pugacheva, and E.A. Golemis. 2012. Calmodulin activation of Aurora-A kinase (AURKA) is required during ciliary disassembly and in mitosis. *Mol. Biol. Cell*. 23:2658–2670. <https://doi.org/10.1091/mbc.e11-12-1056>
- Plotnikova, O.V., S. Seo, D.L. Cottle, S. Conduit, S. Hakim, J.M. Dyson, C.A. Mitchell, and I.M. Smyth. 2015. INPP5E interacts with AURKA, linking phosphoinositide signaling to primary cilium stability. *J. Cell Sci.* 128: 364–372. <https://doi.org/10.1242/jcs.161323>
- Pugacheva, E.N., S.A. Jablonski, T.R. Hartman, E.P. Henske, and E.A. Golemis. 2007. HEF1-dependent Aurora A activation induces disassembly of the primary cilium. *Cell*. 129:1351–1363. <https://doi.org/10.1016/j.cell.2007.04.035>
- Ran, J., Y. Yang, D. Li, M. Liu, and J. Zhou. 2015. Deacetylation of α-tubulin and cortactin is required for HDAC6 to trigger ciliary disassembly. *Sci. Rep.* 5:12917. <https://doi.org/10.1038/srep12917>
- Rawlins, L.E., H. Jones, O. Wenger, M. Aye, J. Fasham, G.V. Harlalka, B.A. Chioza, A. Miron, S. Ellard, M. Wakeling, et al. 2019. An Amish founder variant consolidates disruption of CEP55 as a cause of hydranencephaly and renal dysplasia. *Eur. J. Hum. Genet.* 27:657–662. <https://doi.org/10.1038/s41431-018-0306-0>

- Rowitch, D.H., B. St-Jacques, S.M. Lee, J.D. Flax, E.Y. Snyder, and A.P. McMahon. 1999. Sonic hedgehog regulates proliferation and inhibits differentiation of CNS precursor cells. *J. Neurosci.* 19:8954–8965. <https://doi.org/10.1523/JNEUROSCI.19-20-08954.1999>
- Sánchez, I., and B.D. Dynlacht. 2016. Cilium assembly and disassembly. *Nat. Cell Biol.* 18:711–717. <https://doi.org/10.1038/ncb3370>
- Seo, S., L.M. Baye, N.P. Schulz, J.S. Beck, Q. Zhang, D.C. Slusarski, and V.C. Sheffield. 2010. BBS6, BBS10, and BBS12 form a complex with CCT/TRiC family chaperonins and mediate BBSome assembly. *Proc. Natl. Acad. Sci. USA.* 107:1488–1493. <https://doi.org/10.1073/pnas.0910268107>
- Spalluto, C., D.I. Wilson, and T. Hearn. 2012. Nek2 localises to the distal portion of the mother centriole/basal body and is required for timely cilium disassembly at the G2/M transition. *Eur. J. Cell Biol.* 91(9): 675–686. <https://doi.org/10.1016/j.ejcb.2012.03.009>
- Spassky, N., F.T. Merkle, N. Flames, A.D. Tramontin, J.M. García-Verdugo, and A. Alvarez-Buylla. 2005. Adult ependymal cells are postmitotic and are derived from radial glial cells during embryogenesis. *J. Neurosci.* 25: 10–18. <https://doi.org/10.1523/JNEUROSCI.1108-04.2005>
- Spiess, C., A.S. Meyer, S. Reissmann, and J. Frydman. 2004. Mechanism of the eukaryotic chaperonin: protein folding in the chamber of secrets. *Trends Cell Biol.* 14:598–604. <https://doi.org/10.1016/j.tcb.2004.09.015>
- Tissir, F., Y. Qu, M. Montcouquiol, L. Zhou, K. Komatsu, D. Shi, T. Fujimori, J. Labeau, D. Tyteca, P. Courtoy, et al. 2010. Lack of cadherins Celsr2 and Celsr3 impairs ependymal ciliogenesis, leading to fatal hydrocephalus. *Nat. Neurosci.* 13:700–707. <https://doi.org/10.1038/nn.2555>
- Valente, E.M., C.V. Logan, S. Mougou-Zerelli, J.H. Lee, J.L. Silhavy, F. Brancati, M. Iannicelli, L. Travaglini, S. Romani, B. Illi, et al. 2010. Mutations in TMEM216 perturb ciliogenesis and cause Joubert, Meckel and related syndromes. *Nat. Genet.* 42:619–625. <https://doi.org/10.1038/ng.594>
- Vogel, T.W., C.S. Carter, K. Abode-Iyamah, Q. Zhang, and S. Robinson. 2012. The role of primary cilia in the pathophysiology of neural tube defects. *Neurosurg. Focus.* 33:E2. <https://doi.org/10.3171/2012.6.FOCUS12222>
- Williams, C.L., C. Li, K. Kida, P.N. Inglis, S. Mohan, L. Semenec, N.J. Bialas, R.M. Stupay, N. Chen, O.E. Blacque, et al. 2011. MKS and NPHP modules cooperate to establish basal body/transition zone membrane associations and ciliary gate function during ciliogenesis. *J. Cell Biol.* 192: 1023–1041. <https://doi.org/10.1083/jcb.201012116>
- Won, J., C. Marín de Evsikova, R.S. Smith, W.L. Hicks, M.M. Edwards, C. Longo-Guess, T. Li, J.K. Naggert, and P.M. Nishina. 2011. NPHP4 is necessary for normal photoreceptor ribbon synapse maintenance and outer segment formation, and for sperm development. *Hum. Mol. Genet.* 20:482–496. <https://doi.org/10.1093/hmg/ddq494>
- Youn, Y.H., and Y.G. Han. 2018. Primary Cilia in Brain Development and Diseases. *Am. J. Pathol.* 188:11–22. <https://doi.org/10.1016/j.ajpath.2017.08.031>

Supplemental material

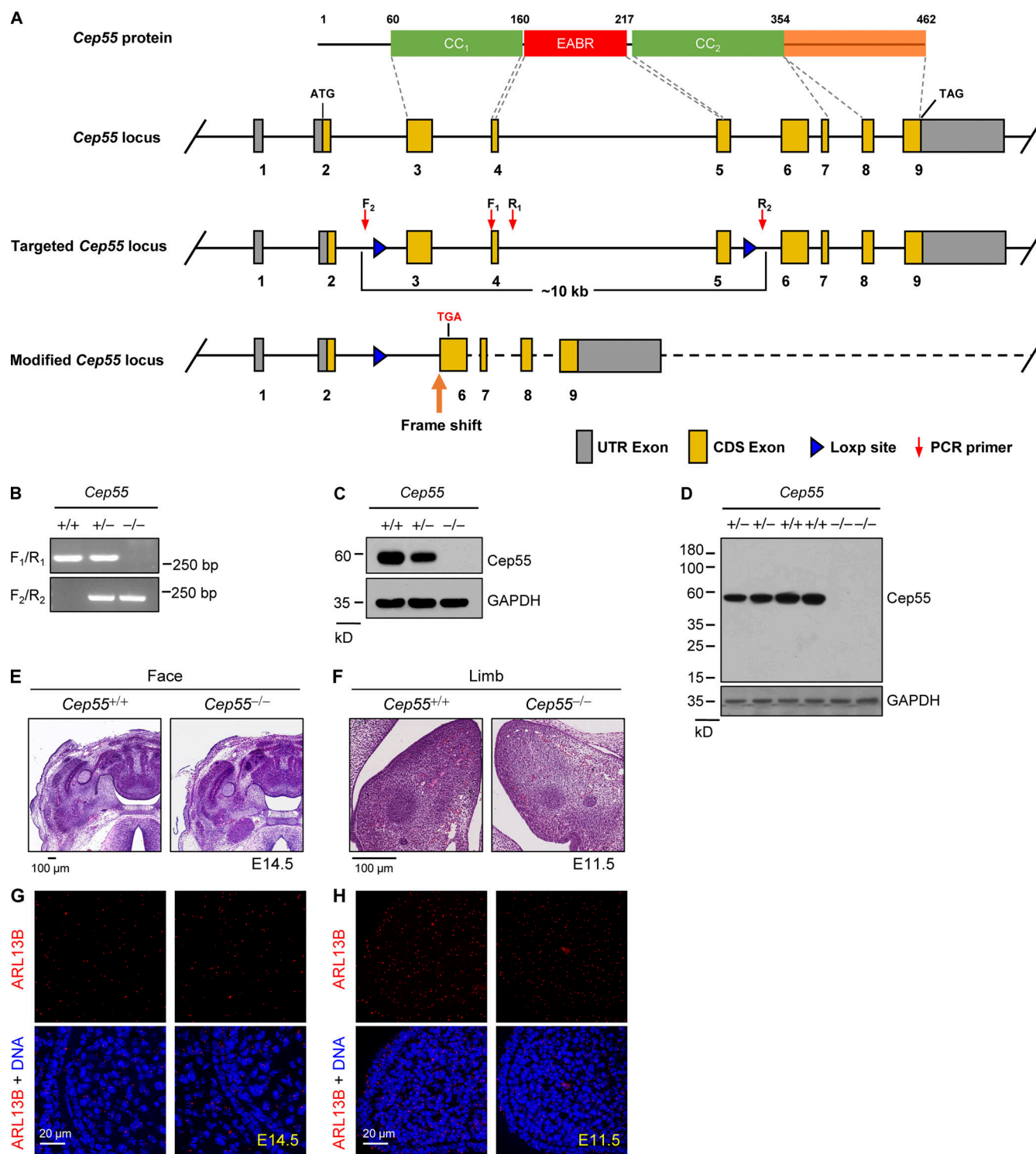


Figure S1. Targeted disruption of the *Cep55* gene in mice, and phenotypes of the face and limb from *Cep55*^{+/+} and *Cep55*^{-/-} mice, related to Fig. 1. (A) Generation of *Cep55*^{-/-} mice. Strategy used to target the mouse *Cep55* locus with CRISPR-Cas9 system. Schematic representation of mouse *Cep55* protein (1–462 aa) and *Cep55* genomic locus. The correlation between *Cep55* functional domains and their coding regions is also indicated (CC₁, CC₂, coiled-coil domain [green]; EABR [ESCRT and ALIX-binding domain, red]; and C-terminal region involved in localization [orange]). Modified *Cep55* locus indicated excision of the genomic region from exon3 to exon5 and formation of a frameshift. Red arrows indicate PCR primers used to verify the null allele. UTR, untranslated region; CDS, coding sequence. **(B)** Genotype analysis of mouse tails from *Cep55* wild-type, heterozygous, and null pups at P0.5. Primers F₁ and R₁ amplify a 300-bp fragment in *Cep55*^{+/+} and *Cep55*^{+/-} pups. Primers F₂ and R₂ amplify a 244-bp fragment in *Cep55*^{+/-} and *Cep55*^{-/-} pups. **(C and D)** Immunoblot analysis of protein extracts from *Cep55*^{+/+}, *Cep55*^{+/-}, and *Cep55*^{-/-} primary MEFs by using anti-Cep55 antibodies produced by Cell Signaling Technologies (C) and Abnova (D). GAPDH was used as a loading control. **(E and F)** Sections of E14.5 faces (E) or E11.5 limbs (F) were stained with hematoxylin and eosin. Scale bars, 100 μ m. **(G and H)** Sections of E14.5 faces (G) or E11.5 limbs (H) from *Cep55*^{+/+} and *Cep55*^{-/-} mice were stained with a ciliary marker (ARL13B, red) and DNA (blue). Scale bars, 20 μ m.

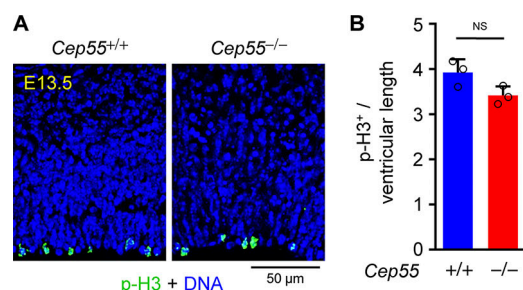


Figure S2. **Cep55 deficiency does not affect the mitotic progression in cerebral cortex, related to Fig. 2.** (A) E13.5 *Cep55*^{+/+} and *Cep55*^{-/-} cerebral cortex coronal sections were stained with mitotic marker (p-H3, green) and DNA (blue). Scale bar, 50 μm. (B) Percentage of p-H3-positive (p-H3⁺) cells in the cerebral cortex in A, calculated per unit ventricle length (100 μm). *n* = 3 embryos each. Data are presented as means ± SD of three independent experiments. An unpaired two-tailed *t* test was performed.

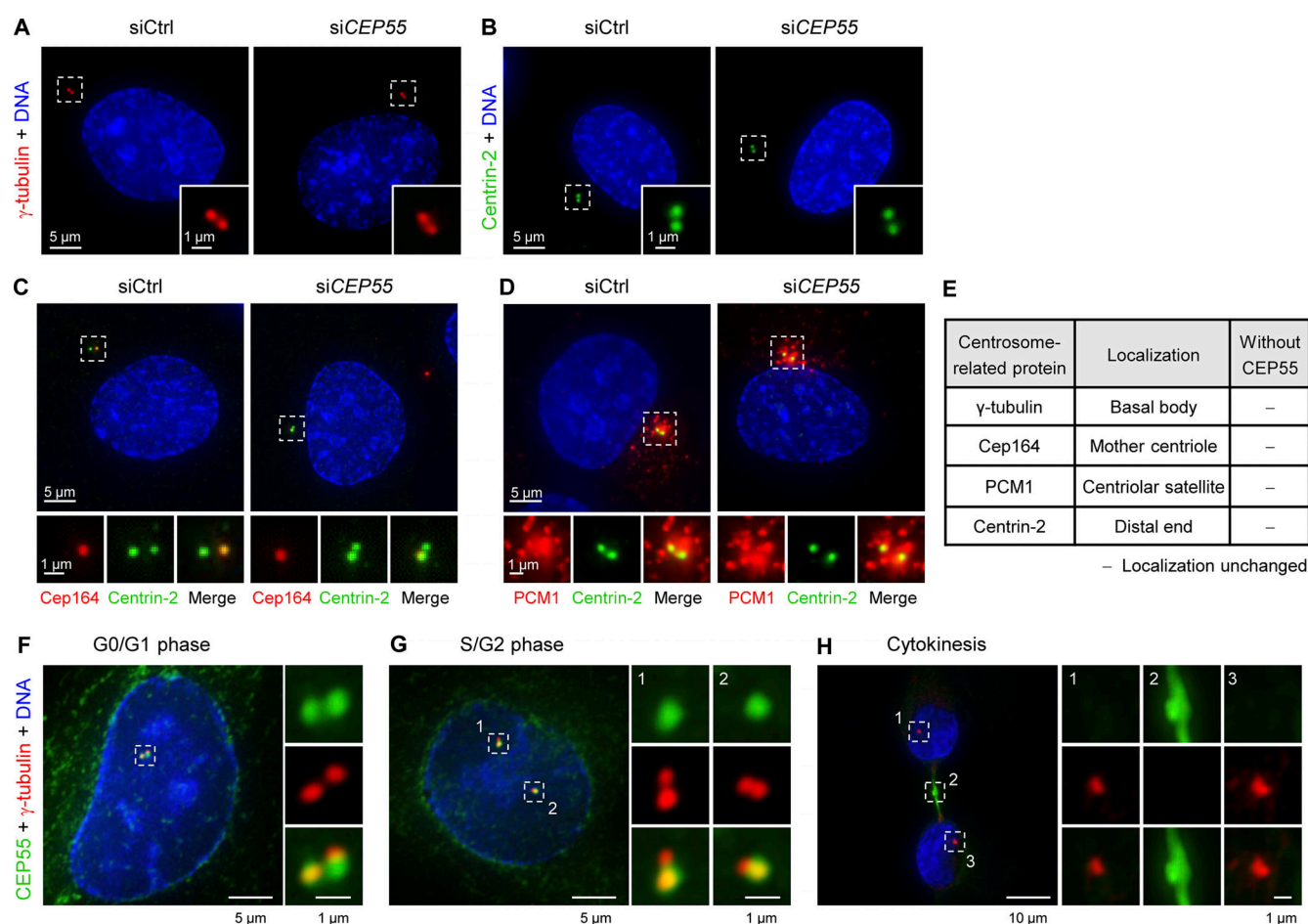


Figure S3. **CEP55 is dispensable for the centrosome integrity and its localization in different cell cycle stages, related to Fig. 3.** (A–D) RPE-1 cells were transfected with control or *CEP55* siRNA in the presence of serum and then stained with indicated antibodies. The localization of γ-tubulin (A, red), Centrin-2 (B–D, green), Cep164 (C, red), and PCM1 (D, red) was not affected by CEP55 depletion. Insets show zoomed-in views of the boxed regions. Scale bars, 5 μm (main image) and 1 μm (magnified region). (E) A table summarizing the centrosome localization of the tested proteins in CEP55-depleted RPE-1 cells. (F–H) Asynchronously growing RPE-1 cells were stained with endogenous CEP55 (green), γ-tubulin (red), and DNA (blue). Representative cells from different stages of the cell cycle are shown. Insets show zoomed-in views of the boxed regions. Scale bars in F and G, 5 μm (main image) and 1 μm (magnified region). Scale bars in H, 10 μm (main image) and 1 μm (magnified region).

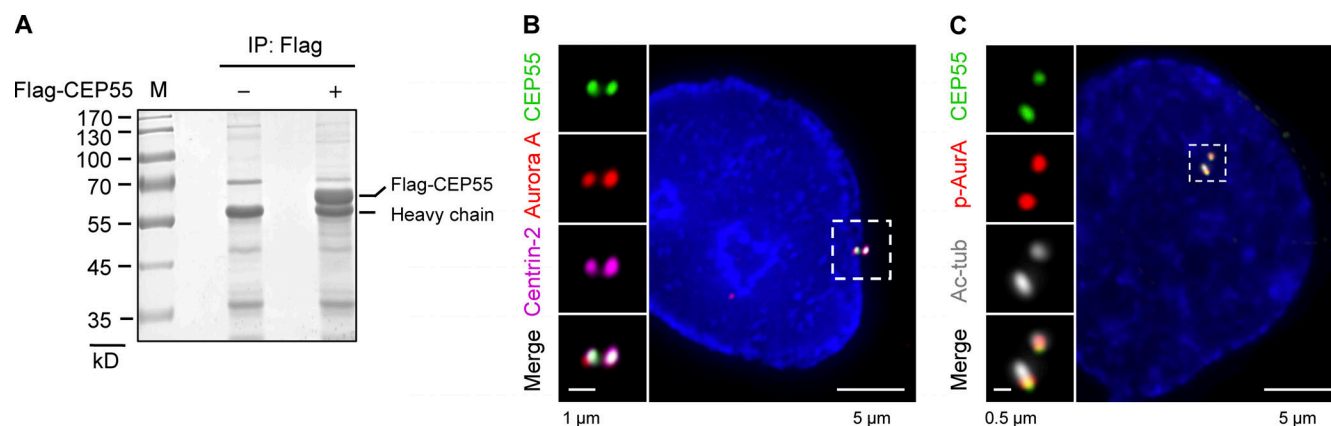


Figure S4. **CEP55 interacts with Aurora A and localizes at the centrosome, related to Fig. 4.** (A) Eluates from representative Flag-vector and Flag-CEP55 immunoaffinity purification experiments were stained with Coomassie blue and subjected to mass spectrometric sequencing. M, marker. (B) CEP55 (green) and Aurora A (red) were costained with a centriolar distal marker (centrin-2, purple) and DNA (blue). Insets show zoomed-in views of the boxed regions. Scale bars, 5 μ m (main image) and 1 μ m (magnified region). (C) RPE-1 cells were starved for 48 h. The ciliated cells were then stimulated with serum for 2 h and stained with CEP55 (green), p-Aurora A (red), Ac-tubulin (gray), and DNA (blue). Insets show zoomed-in views of the boxed regions. Scale bars, 5 μ m (main image) and 0.5 μ m (magnified region).

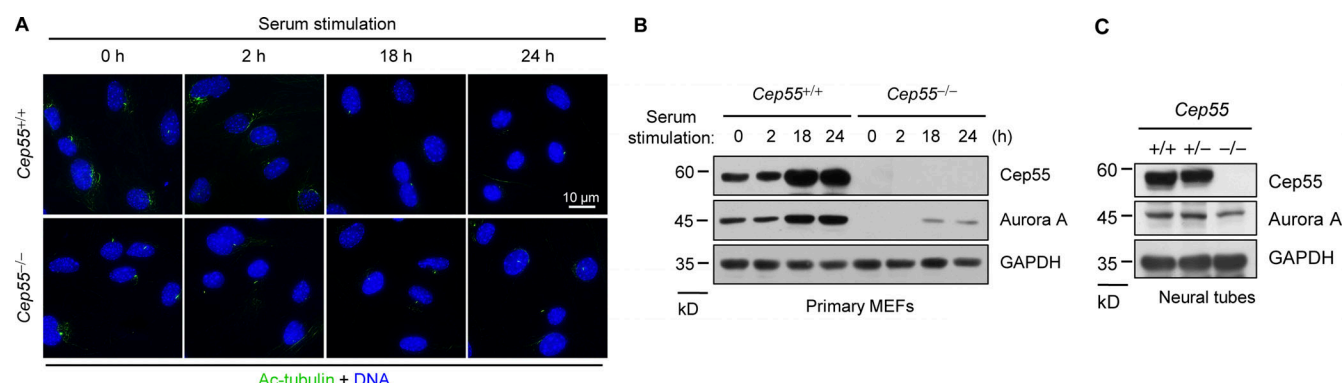


Figure S5. **Cep55 deficiency inhibits cilia disassembly and the stability of Aurora A protein in primary MEFs, related to Fig. 5.** (A) Cep55^{+/+} and Cep55^{-/-} primary MEFs were starved for 48 h. The ciliated primary MEFs were then stimulated with serum for the indicated times and stained with Ac-tubulin (green) and DNA (blue). Scale bar, 10 μ m. (B) Cell lysates in A were detected with the indicated antibodies. (C) Immunoblot analysis with anti-Cep55 and anti-Aurora A antibody on protein extracts from E9.5 Cep55^{+/+}, Cep55^{+/-}, and Cep55^{-/-} neural tubes. GAPDH was used as a loading control.

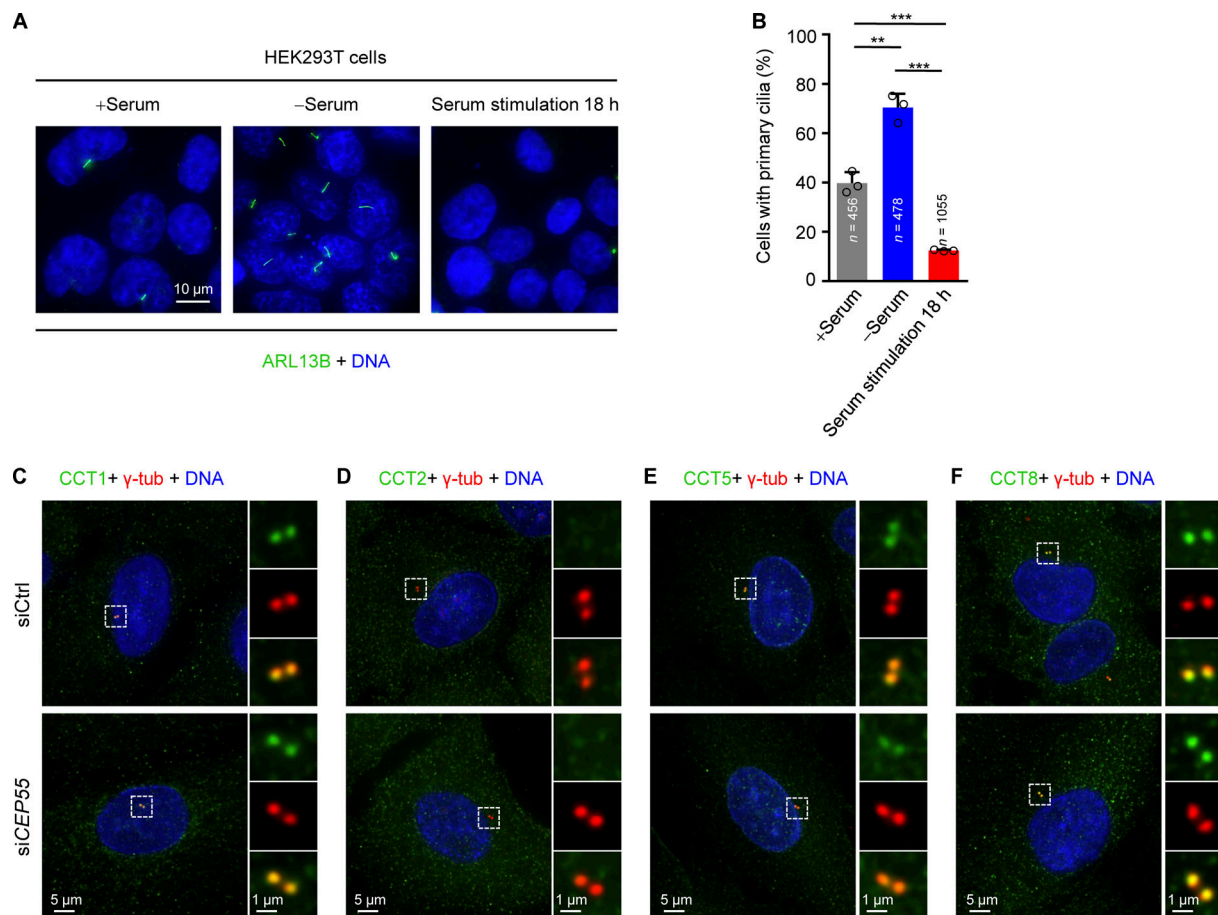


Figure S6. **Cilia assembly and disassembly in HEK293T cells and the localization of CCT proteins in CEP55-depleted cells, related to Fig. 6. (A)** HEK293T cells were starved for 48 h. Ciliated cells were then stimulated with serum for 18 h and stained with ARL13B (green) and DNA (blue). Scale bar, 10 μ m. **(B)** Quantification of the ciliated cells in A. Data are presented as means \pm SD of three independent experiments. A one-way ANOVA test was performed. ***, $P < 0.001$. n , number of cells. **(C–F)** RPE-1 cells transfected with control or CEP55 siRNA were stained with CCT proteins (green), γ -tubulin (red), and DNA (blue; CCT1 in C, CCT2 in D, CCT5 in E, and CCT8 in F). Insets show zoomed-in views of the boxed regions. Scale bars, 5 μ m (main image) and 1 μ m (magnified region).

Table S1 is provided online and shows the genotype distributions of offspring of *Cep55* heterozygous mice intercrossed at different ages.